POLITECNICO DI MILANO

SCHOOL OF CIVIL, ENVIRONMENTAL AND LAND MANAGEMENT ENGINEERING

MSc. GEOINFORMATICS ENGINEERING

FWLANDSAT5: NEW MONITORING SYSTEM OF FRESHWATER USING LANDSAT 5 IMAGES

Supervisor:

Prof. Giovanna Venuti

Co-supervisor:

María Jesús García (Universidad Politécnica de Madrid)

José Antonio Domínguez (Crop Research Institute of Czech Republic)

Master graduation thesis by:

Lady Carolina Echavarría Caballero

Matri. 873389

Thesis Work developed within the framework of the Erasmus agreement with Universidad Politécnica de Madrid.

Academic year 2017/2018

ABSTRACT

Since 1949 mining activity has been performed between the lower courses of the Manzanares and Jarama rivers in Madrid (Spain) and it has resulted in the generation of gravel pit ponds due to outcrop of the phreatic level when the dredging is done. In 1994, this zone was declared as a protected area and recognized as “Parque Regional del Sureste” (PRSE). The main purpose of the natural park declaration is to protect this area against all kind of negative environmental impact, having as a result the monitoring and control measures of gravel extraction. The use of remotely sensed data is proposed as a tool for monitoring these water bodies.

The main objective of the current work is to assess the use of Landsat TM5 images which have been atmospherically corrected with software called Landsat Ecosystem Disturbance Adaptive Processing System (LEDAPS) developed by the United State Geological Survey (USGS) for studying water quality time series, using water leaving reflectance measured in the field. The high number of Landsat 5 images used in this project has required to develop several scripts in Python with which a new monitoring system of freshwater been have built, which name is FWLandsat5.

To achieve this, first the Normalized Difference Water Index (NDWI) has been applied to 230 available Landsat5-TM images of the area under consideration (scene Path 201 and Row 32) from years 1984 to 2011 to distinguish water and non-water information. Moreover, the Landsat Surface Reflectance was compared with available water spectral reflectance showing a significantly overestimation of Landsat surface reflectance. Thus, a new regression equation with the Secchi Disk *in situ* measurements and reflectance measured in the sensor bands should be retrieved and validated.

Then, the retrieved Secchi disk (SD) model is applied to every image providing a value for each pixel of the SD for every image over the time series. Finally, the Inventory of water bodies in the natural park is carried out, as well as the identification of its trophic state based on the OECD classification and the monitoring of the ecological status of the water bodies according to the European Water Framework Directive (WFD).

The area composed by water bodies in PRSE had an increasing period from 1984 to 2006 but it is not visible any seasonal trend. For its part, it is possible to identify a SD seasonal behavior, where the highest SD values are present in the winter (January and December) while the lowest values during summer (August), which corresponds with the phytoplankton growth. It is also evident the improvement of water quality over time, having both the trophic state of the water bodies based on the OECD classification and the Ecological Quality Ratio (EQR) according to the WFD.

RIASSUNTO

Dal 1949, si è sviluppata l'attività mineraria tra la zona inferiore dei fiumi Manzanares e Jarama a Madrid (Spagna), con la conseguente generazione di laghi cava di ghiaia a causa della risalita della livello freatico, quando il dragaggio è fatto. Nel 1994, questa zona è stata dichiarata area protetta e riconosciuta come "Parque Regional del Sureste" (PRSE). Lo scopo principale della dichiarazione della riserva naturale è quello di proteggere questa zona contro ogni tipo di impatto ambientale negativo, con conseguente misure di monitoraggio e controllo dell'estrazione di ghiaia. L'uso di dati derivati dal telerilevamento è stato proposto come strumento per monitorare questi corpi idrici.

L'obiettivo principale di questo lavoro è quello di valutare l'uso delle immagini Landsat TM5 Atmosfericamente corretto con il modello denominato " Landsat Ecosystem Disturbance Adaptive Processing System" (LEDAPS), sviluppato dalla United States Geological Survey (USGS) per studiare serie temporanee di qualità dell'acqua, utilizzando i valori di riflettanza misurati sul campo. L'elevato numero di immagini Landsat 5 utilizzate in questo progetto ha richiesto lo sviluppo di diversi script Python con cui è stato creato un nuovo sistema di monitoraggio dell'acqua dolce, il cui nome è FWLandsat5.

Per raggiungere questo obiettivo, il “Normalized Difference Water Index” (NDWI) è stato inizialmente applicato a 230 immagini Landsat5-TM disponibili nell'area di studio (scena: colonna 201 e riga 32) dal 1984 al 2011, per discriminare le zone di acqua e non di acqua. Inoltre, la riflettanza superficiale di Landsat è stata confrontata con la riflettanza spettrale dell'acqua misurata nel campo, determinando una sovrastima significativa della riflettanza della superficie di Landsat. Pertanto, è stato necessario ottenere e convalidare una nuova equazione di regressione dalle misurazioni del Disco Secchi (DS) *in situ* e la riflettanza misurata nelle bande del sensore.

Successivamente, il modello DS ottenuto viene applicato alle immagini per fornire un valore DS per ciascun pixel in tutte le serie temporali. Infine, abbiamo effettuato un inventario dei corpi idrici nel parco naturale e per identificare lo stato trofico sulla base della classificazione Organizzazione per la Cooperazione e lo Sviluppo (OESE) e monitoraggio dello stato ecologico dei corpi idrici secondo la Direttiva Quadro sulle Acque dell’Unione europea (DQA).

L'area composta da corpi idrici nel PRSE ha avuto un periodo crescente dal 1984 al 2006, ma non è possibile identificare eventuali tendenze stagionali. Nel frattempo, è possibile individuare un comportamento stagionale dei DS, in cui i valori più alti si trovano in inverno (gennaio-dicembre) ei valori più bassi osservati durante l'estate (agosto), che corrispondono a una crescita del fitoplancton. Anche il miglioramento della qualità dell'acqua nel tempo è evidente, sia nello stato trofico delle masse d'acqua secondo la classificazione OCSE che nel “Ecological Quality Ratio" (EQR) secondo la DQA.

ACKNOWLEDGEMENT

I would first like to thank my thesis advisors Maria Jesús Garcia of Universidad Politécnica de Madrid and José Antonio Dominguez of Crop Research Institute of Czech Republic. The door of Prof. Garcia office was always open, as well as a prompt answer from Prof. Dominguez whenever I ran into a trouble spot or had a question about my research or writing. They always steered me in the right the direction.

I would also like to thank Dr. Miguel Álvarez Cobelas (Spanish National Research Council - CSIC), the expert who provided me the Secchi disk data and valuable developed researches to support my thesis work.

Finally, I must express my very profound gratitude to my parents and to my boyfriend for providing me with unfailing support and continuous encouragement during the development of this thesis. This accomplishment would not have been possible without them.

Thank you.

Carolina Echavarria Caballero

TABLE OF CONTENTS

LIST OF FIGURES

LIST OF TABLES

1 INTRODUCTION

1.1 Interaction of atmosphere and electromagnetic radiation

Before the sun radiation reaches the earth surface, three relevant interactions in the atmosphere take place (Bakker, et al., 2009):

- **Absorption:** The process in which electromagnetic energy is converted into other forms of energy (e.g. heat or fluorescence) or causing chemical reactions (such as photosynthesis).
- **Transmission**: The procedure of passing on energy through a medium or material.
- **Scattering:** A general physical process in which some forms of radiation are forced to deviate from a straight trajectory by one or more localized non-uniformities in the medium through which they pass.

Electromagnetic (EM) radiation that propagates through the atmosphere is partly absorbed by molecules. The strongest absorbers of solar radiation in the atmosphere are ozone (O3), water vapor (H_2O), and carbon dioxide (CO_2). Many wavelengths are not useful for remote sensing of the earth surface, given the high absorption levels (Figure 1). The useful ranges are referred to as the atmospheric transmission windows (Bakker, et al., 2009; Shaw & Nugent, 2013).

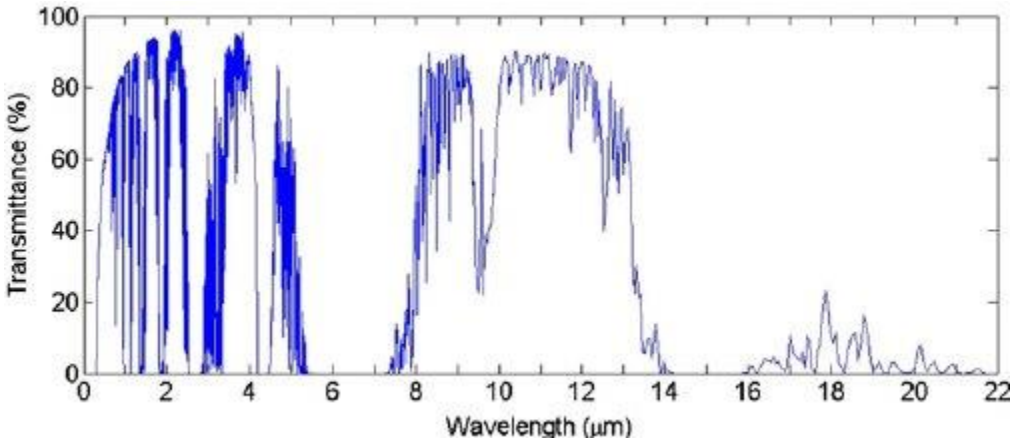

Figure 1. Atmospheric transmittance versus wavelength, calculated with Modtran5 for a zenith (Shaw & Nugent, 2013)

1.2 Energy interaction with the earth surface

Spectral regions with high transmission or atmospheric windows include: Ultraviolet 0 – 0.4µm, the visible (~0.4–0.7µm), short-wave infrared (SWIR~1–2µm), mid-wave infrared (MWIR~3–5µm), and long-wave infrared (LWIR~8–14µm). The MWIR window is interrupted by carbon dioxide absorption centered at 4.3µm and the LWIR window has ozone absorption centered at 9.6µm (Shaw & Nugent, 2013).

Different surface types such as water, bare ground and vegetation reflect radiation differently in various channels. The radiation reflected as a function of the wavelength is called the spectral signature of the surface (Figure 2).

The spectral reflectance curve of healthy green vegetation has a significant minimum of reflectance in the visible portion of the electromagnetic spectrum (band 3 of Landsat) resulting from the pigments in plant leaves. Reflectance increases dramatically in the near infrared (band 4). Stressed vegetation can also be detected because stressed vegetation has a significantly lower reflectance in the infrared (Patel, et al., 1982).

The reflection from bare ground increases slightly from the visible to the infrared range of the spectrum. There are great differences between different types of soil, dry and humid land. Different mineral compositions of the surface are also reflected in the spectral signature (Govender, et al., 2007).

Generally, water only reflects in the visible light range. As water has almost no reflection in the near infrared range it is very distinct from other surfaces. Water surfaces will therefore be clearly delimited as dark areas (low pixel values) in images recorded in the near infrared range (Bakker, et al., 2009).

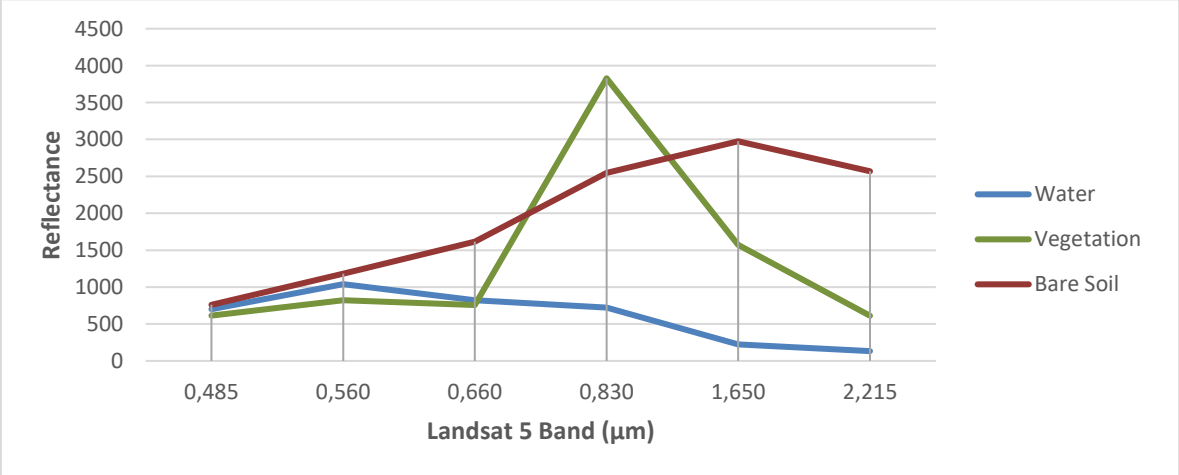

Figure 2. Spectral signatures of soil, vegetation and water and spectral bands of Landsat 5.

Sediment, suspended material and algae in water will affect the spectral response curve. Thus, the turbid water achieves the highest reflectance and the water containing plants has a reflectance peak for the green light because of the chlorophyll of the plants (Figure 3).

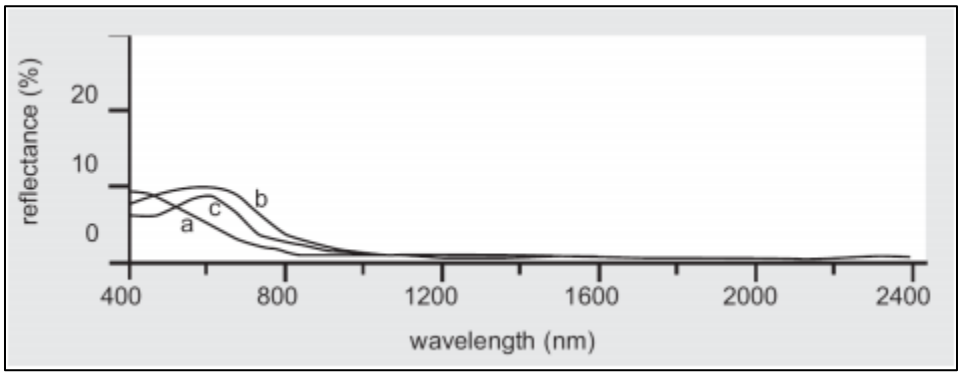

Figure 3. Water reflectance. a) Ocean water, b) turbid water, c) water with chlorophyll. (Bakker, et al., 2009)

1.3 Background of inland waters remote sensing.

Remote sensing, in general, analyses radiation measured by a distant sensor to derive information of a certain object in the optical, thermal and radar ranges. In case of the water bodies, the remote sensing obtains information from two types of radiance: thermal radiance and water leaving radiance. Thermal radiance allows to determinate the superficial temperature (Singh, et al., 2018) and water leaving radiance enable to study water properties such as transparency, biota, bathymetry, etc. (Dörnhöfer & Oppelt, 2016).

To obtain information on lake properties such as water transparency, the water leaving radiance in the visible and near-infrared wavelengths, i.e. the wavelength region where water reflects and scatters most of the incoming solar radiation (400–900 nm) is of major interest (Dörnhöfer & Oppelt, 2016).

Before the incident solar radiation interacts with the water body, it has to pass the atmosphere where it is modified by absorption and scattering. At the water surface radiation is either reflected or it passes the water surface, and further propagates through the water body. In the water column, optically active constituents (e.g. SPM, CDOM and Chl-a) alter radiation by absorption and scattering characteristic for each constituent. Finally, by passing

the water surface, the water leaving radiation is again refracted and, through its way towards the satellite sensor, is affected once more by atmospheric absorption and scattering (Dörnhöfer & Oppelt, 2016).

Under most circumstances, over 90% of the light reaching a satellite over an aquatic target derives from the atmosphere. Therefore, the largest potential source of error and uncertainty in measuring from space is the residual error from atmospheric correction. For that reason, an accurate removal of effects due to the atmosphere and water surface is essential (Mouw, et al., 2015).

Separation of the various contributors from the water leaving radiance allows to obtain quantitative information on water constituents (e.g. SPM, CDOM, phytoplankton or cyanobacteria) and, for shallow water, bathymetry and bottom substrate (e.g. benthic vegetation, sediment).

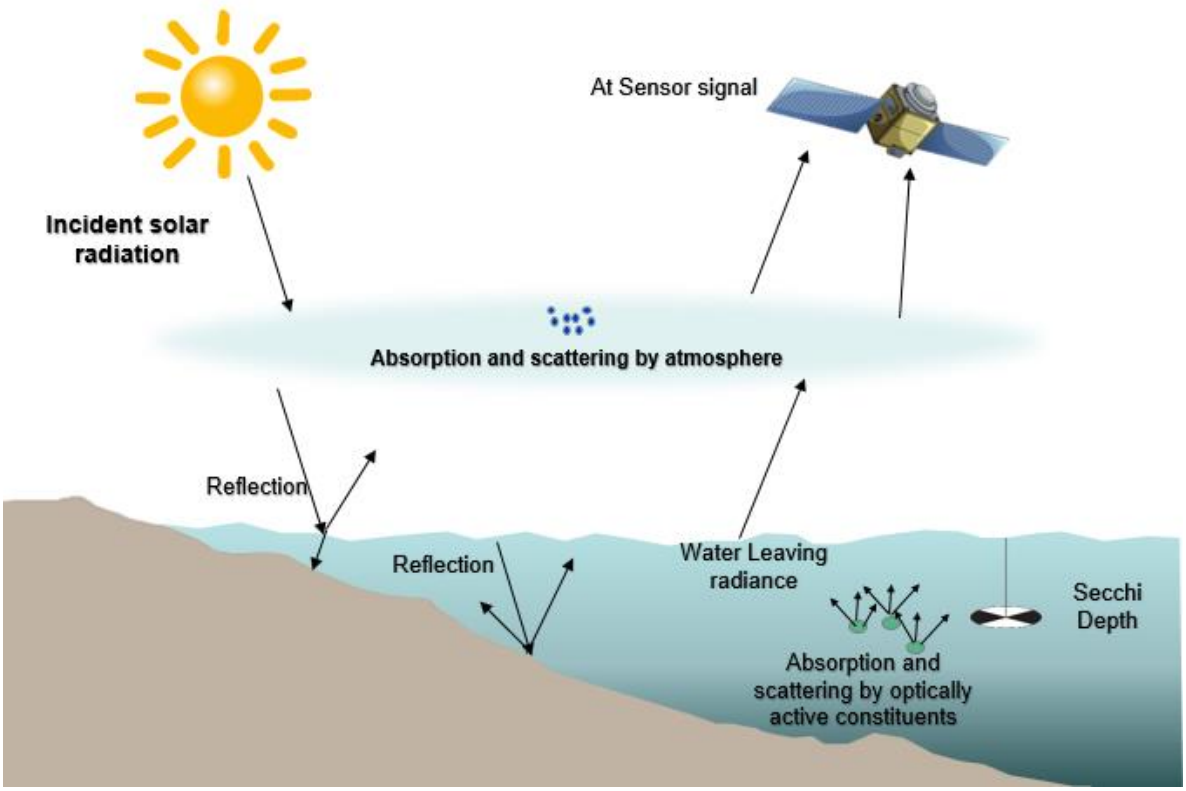

Figure 4. Interaction between radiation, remote sensing indicators of lake ecology and sensors. Adapted from Dörnhöfer & Oppelt, (2016).

1.4 Atmospheric correction methods

Atmospheric correction is a process in which the top-of-atmosphere radiance received by sensors is converted to surface reflectance.

At satellite radiance must be converted to surface reflectance by correcting for both solar and atmospheric effects. The general model/equation used to do this is (Moran, et al., 1992):

$$REF = \frac{(PI \ * (Lsat \ - Lhaze))}{(TAUv * (E0 \ * Cos\,(Tz) * TAUz \ + Edown))} \quad (1)$$

REF: Spectral reflectance of the surface

$Lhaze$ *: Upwelling atmospheric spectral radiance scattered*

$TAUv$: *Atmospheric transmittance along the path from the ground surface to the sensor.*

$E0$: *Solar spectral irradiance*

Tz: *Angle of incidence*

$TAUz$: *Atmospheric transmittance along the path from the sun to the ground surface.*

All radiometric correction procedures start with this general model but make different simplifying assumptions that eliminate certain parameters:

1.4.1 Dark object subtraction (DOS).

The image based dark object subtraction (DOS) model has the basic assumption that within the image, some pixels are in complete shadow and their radiances received at the satellite are due to atmospheric scattering. The objective is to select spectral band haze values that are collected from the digital image. Therefore, in the general model shown in equation 1, the following applies for the DOS model:

$Lhaze$: value derived from the digital image using the dark object criteria.

$TAUv$: 1.0 (ignores atmospheric transmittance)

$TAUz$: 1.0 (ignores atmospheric transmittance)

$Edown$: 0.0 (ignores downwelling)

The DOS model main advantages are that it is strictly an image-based procedure and does not require in situ field measurements. The main disadvantages are that for reflectance values greater than about 15 percent the accuracy is often not acceptable and that the selection of the haze values must be done with care (Chavez, 1996).

1.4.2 Cosine of the solar zenith angle correction (COST) Dark Object Subtraction (DOS).

COST is a radiometric calibration method based entirely on the characteristics of the satellite image. Applies Dark Object Subtraction (DOS) to compensate for the additive components of the atmosphere, which mainly affect the shortest wavelengths. For initial estimation of the multiplicative effect, the value of the atmospheric transmittance along the path from the ground to the sensor (TAUz) is computed from the cosine of the solar zenith angle (Song, et al., 2001).

$Lhaze$: *value derived from the digital image using the dark object criteria.*
$TAUv$: *1.0 (ignores atmospheric transmittance)*
$TAUz$: $Cos\ (Tz)$
$Edown$: *0.0 (ignores downwelling)*

1.4.3 Atmospheric Correction for OLI 'lite' – ACOLITE

Atmospheric correction methods that relies on scene information. ACOLITE module was developed by the Royal Belgian Institute of Natural Sciences (RBINS) and allows processing OLI/L8 data quickly and easily, for inland, coastal and oceanic. ACOLITE computes the average values of solar irradiance (E0), Rayleigh optical thickness, ozone thickness, and water absorption (aw) based on the convolution of OLI relative spectral response function. The assumptions and calculations are detailed in Vanhellemont & Ruddick, (2015) that describes the equations used to compute and correct the aerosol and Rayleigh scattering effects.

1.4.4 Second Simulation of the Satellite Signal in the Solar Spectrum correction scheme (6S)

The 6S model is a computer code which can accurately simulate the atmosphere along the path from sun to Target (surface) to sensor. The 6S code is an improved version of 5S, developed by the Laboratoire d'Optique Atmospherique. The 6S version permits calculations of near-nadir (down-looking) aircraft observations, accounting for target elevation, non-Lambertian surface conditions, and new absorbing species (CH4, N2O, CO). The computational accuracy for Rayleigh and aerosol scattering effects has been improved

by the use of state-of-the art approximations and implementation of the successive order of scattering (SOS) algorithm (Vermote, et al., 1997).

1.4.5 Fast Line-of-sight Atmospheric Analysis of Hypercubes – FLAASH;

Physical method which attempts to model the atmospheric effects by solving a radioactive transfer equation. FLAASH is an interface of MODTRAN (MODerate spectral resolution atmospheric TRANsmittance), and its performance depends on input data, such as initial visibility, optical depth, aerosol type model, and water vapor amount (Adler-Golden, et al., 1999)

1.5 Trophic state

Eutrophication is the process by which water bodies are made more eutrophic through an increase in their nutrient supply (Figure 5). This nutrient enrichment can lead to highly undesirable changes in ecosystem structure and function (Smith, et al., 1999).

At the end of the 20th century, the Oslo and Paris Commission (OSPAR) in charge of promoting the good ecological status of West-European coastal seas proposed an operational definition of eutrophication (Oslo and Paris Commission OSPAR , 1997). Eutrophication was then considered as “the result of excessive enrichment of water with nutrients which may cause an increase in the accelerated growth of algae in the water column and higher forms of plants living on the bottom.”

The study of many lakes, first affected by anthropogenic eutrophication in the second half of the 20th century, has shown (Vollenweider, 1968) that eutrophication is possible only if the surface mixed layer is sufficiently thin and illuminated to allow a primary production greater than the algal respiration and hence, to ensure a rapid algal growth. The biomass produced can accumulate only if the water body exhibits a residence time of several days, i.e. is sufficiently confined. Eutrophication in lakes revealed to have been mainly triggered by massive anthropogenic inputs of inorganic phosphorus (phosphate).

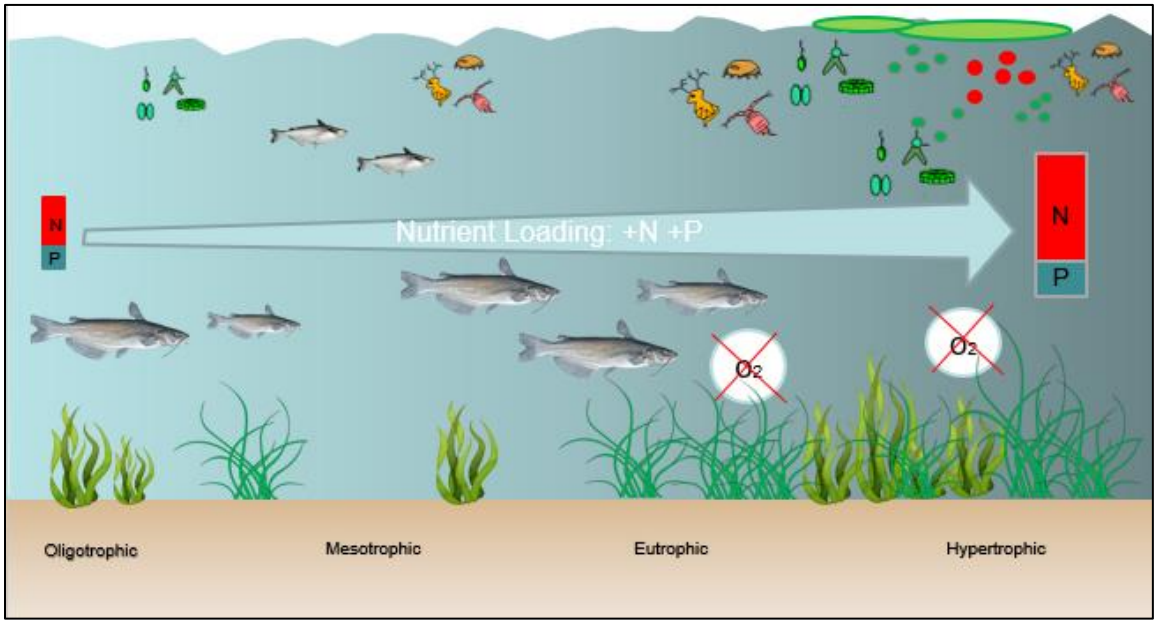

Figure 5. Conceptual schematic showing the progression of a system towards eutrophication with the increased loading of both nitrogen and phosphorus (Glibert, 2017).

The trophic classifications of lakes have a long story and the use of trophic status categories, such as oligotrophic, mesotrophic a eutrophic (or subdivisions thereof) have been widely adopted (Vollenweider, 1968; Smith, et al., 1999; Wetzel, 2001). In the Table 1, the OECD[1] classification is presented (Vollenweider & Kerekes, 1982; Giardino, et al., 2001):

Table 1. Trophic classification of lakes, with their corresponding phosphorus, chlorophyll concentrations and transparency (secchi depth)

Trophic level	Total Phosphorus (µg L^{-1}) (1)	Chlorophyll a (µg L^{-1})		Secchi depth(m)	
		Annual Mean	Annual Max	Annual Mean	Annual Min
Ultra -oligotrophic	< 4	< 1	<2.5	>12	>6
Oligotrophic	4 – 10	<2.5	< 8	>6	>3
Mesotrophic	10 – 35	2.5 - 8	8 - 25	6 – 3	3 – 1.5
Eutrophic	35 – 100	8 - 25	27 - 75	3 – 1.5	1.5 – 0.7
Hypereutrophic	>100	> 25	>75	<1.5	<0.7

(1) Total Phosphorus concentration in the water body

[1] Organization for Economic Co-Operation and Development - OECD research

Until the entry into force of the European Water Framework Directive (WFD), approved in 2001, the OECD classification was used. The WFD requires that all European water bodies are assigned to one of five ecological classes (high, good, moderate, poor, bad) and these classes are defined according to the Ecological Quality Ratio (EQR) (Domínguez Gómez, et al., 2009):

$$EQR = \frac{(Observed\ Ecological\ Value)}{(Reference\ Ecological\ Value)} \qquad (2)$$

However, the directive is not very specific and provides only general guidance on how to define the proposed ecological classes. One of the major and more practical challenges for implementation of the directive is therefore how to define and determine the ecological status of a specific waterbody (Søndergaard, et al., 2005).

According to the WFD the ecological state of a waterbody should be defined relative to its deviation from the reference condition, i.e. the expected ecological quality in the absence of anthropogenic influence. Reference conditions and ecological classifications need to be specified to individual lake types, as different lakes do not necessarily respond similarly to a stress factor such as, for instance, eutrophication.

Domínguez Gómez, et al., (2009) choose the transparency as parameter to determine the EQR when using remote sensing and the reference ecological value chosen is SD = 5 m because the maximum SD measured in the field data is 4.30 m. They considered 5m to be the suitable reference ecological value bearing in mind previous research, such as the study in deep Danish lakes in which the EQR used for the ecological classification of these lakes was SD>5.1m (Søndergaard, et al., 2005).

The EQR categorization for the water bodies was done following the classification of Søndergaard, et al., (2005): bad, 0–0.2; poor, 0.2–0.4; moderate, 0.4–0.6; good, 0.6–0.8; and high, .0.8.

1.6 Background and context

The area between low course of rivers Manzanares and Jarama, after several years of intense gravel extraction activity, was designated as natural park “Parque Regional del Sureste” in 1994[2]. The main purpose of the natural park declaration is to protect this area against all kind of negative environmental impact, having as a result the prohibition of gravel

[2] Official Bulletin of Madrid – BODM 163, July 12th, 1994

extraction. This activity has resulted in the generation of gravel pit ponds due to outcrop of the phreatic level when the dredging is done, these artificial ponds, when abandoned, turned into wetland ecosystems with an established aquatic fauna and flora (Domínguez Gómez & Peña, 1999).

Since European Water Framework Directive was approved, all the European Communities have the responsibility of supervising the quality of the water bodies (European Commission, 2000), but not enough resources are available to carry out only field data methodologies in all the water bodies. Thus, to improve the spatial and temporal monitor and management of water resources is necessary to make use of new technologies as remote sensing systems. Satellite imagery offers the opportunity to extend low-cost monitoring and to examine spatial and temporal variability in water clarity data (Hicks, et al., 2013).

The state of an ecosystem can be characterized by a set of ecosystem indicators such as environmental, biophysical, ecological, and social attributes. Many of these ecosystem attributes, if not all, can be measured, assessed, and monitored by remote sensing and their states and trajectories can be quantified, analyzed, and even projected for sustainable planning, development, and intervention, if needed (Qi, et al., 2017).

The trophic state of water bodies has been studied for years. Eutrophication is the most important worldwide environmental issue regarding reservoirs and many other types of aquatic ecosystems and is responsible for water quality degradation and severe restriction in water uses (Padedda, et al., 2017).

In particular, water transparency is an essential lake property on water quality (Domínguez Gómez, et al., 2009; Dörnhöfer & Oppelt, 2016; Soria, et al., 2017), because it gives a general view of all the water components and the interaction among them. This is the reason why transparency is included in the quality elements for the classification of ecological status in the European Communities (European Commission, 2000). Among different methods, the Secchi disk (SD) is the oldest “optical instrument” used to measure transparency of ocean and lake waters due to its low cost and easiness to operate. SD is a white or black-and-white disk with a diameter generally about 30 cm, that is lowered into a water body until it is no longer viewable by an observer (Rudolph W., 1986; Wernand, 2010; Lee, et al., 2015).

Moreover, remote sensing of water quality has already been studied for quite some time using the spectral reflectance: for example, water quality predictive regression equations to

monitor the year-to-year spatial variation of trophic zones by Secchi transparency and chlorophyll a concentration in US lakes was developed by Verdin, (1985). The assessment of Landsat TM capabilities in retrieving seston dry weight, sum of chl-a and phaeopigments and Secchi depth in a Dutch lake has been carried out by Dekker & Peters, (1993). Also, an integration of remote sensing data (Landsat 5 and SPOT-HRV), in situ data and water quality models for the assessment of suspended matter concentrations in the southern Frisian lakes in the Netherlands was done by Dekker, et al., (2001). Meanwhile, the Taihu Lake, has been studied with the aim of deriving a model for the retrieval of suspended sediment (SS) concentrations from Landsat TM images and in situ sampled data (Guang, et al., 2006). Additionally, the evaluation of the suitability of Landsat archive for mapping Colored dissolved organic matter (CDOM) changes in Swedish lakes over the last 30 years (Kutser, 2012).

In Spain, remote sensing techniques have been used to estimate water quality variables such as chlorophyll-a, total suspended particles and water transparency (Doña, et al., 2014). In 1997 the university of Alcalá and CEDEX carried out the environmental impact assessment of extracting activities and limnological surveys of several water bodies in the river Tajo basin making use of Landsat TM imagery. Later, this proposal was joined by Domínguez Gómez & Peña, (1999) in order to assess the trophic state.

Domínguez Gómez, et al., (2009) monitored the transparency in inland bodies from water reflectance field measurement, Landsat TM/ETM+ and Aircraft DS-1268. The researchers sampled ground data of water reflectance, solar irradiance and transparency at different depths having as a result an algorithm for measuring transparency from the most suitable wavelength range corresponding to 520-600 nm. The derived algorithm was used in 2017 for monitoring the water quality of Spanish reservoirs as an adaptation of the methodology used in Landsat 5 images and verified with Landsat 8 data and field data in the Picadas reservoir, from September 2015 to December 2016, allowing the evaluation of the trophic state (Domínguez, et al., 2017).

Meanwhile, an empirical equation for transparency estimation was also derived, evaluated and performed for a set of satellite images from 1984 to 2000, to estimate the spatial variation of transparency by Soria, et al., (2017). Also, Doña, et al., (2014) developed empirical algorithms for the estimation of chlorophyll-a, total suspended particles, and water transparency through simple regression techniques of Landsat TM and ground data from several Spanish lakes ranging from oligotrophic to hypereutrophic. Chlorophyll-a was

obtained with the ratio in reflectance values between bands 2 and 4 of TM, transparency through Secchi Disk from reflectance in band 2 and total suspended particles from reflectance in band 4.

The continentality of the atmosphere over inland waters and their proximity to the land surface also introduce additional difficulties for atmospheric and adjacency correction procedures and this further impacts the performance of in-water algorithms. Improvements are still needed in the methods for the correction of atmosphere and land adjacency effects over inland waters, particularly in the presence of complex aerosols. (Palmer, et al., 2015).

The performance of atmospheric correction is therefore key to quality assured geophysical variables, retrieved from remote sensing reflectance for monitoring water quality, given the high absorption and low scattering properties, representative of water bodies. Thus, radiometric validation is essential to develop accurate remote sensing algorithms, and this is the reason why several authors have assessed multiple atmospheric correction methods (Qin, et al., 2017; Pahlevan, et al., 2017), as indicated in the following table:

Table 2. Researches deducing atmospheric corrections applied in water studies.

Authors	Techniques	Parameters	Study Area	Methodology
Giardino, et al., (2001)	DOS (Chavez, 1996)	Chl a, SD and ST	Sub-alpine Lake Iseo (Italy)	Atmospheric transmittance (TAUz) was measured in synchrony with the satellite passage. Used an empirical approach for relating atmospherically corrected TM spectral reflectance values and in situ measurements collected during the satellite data acquisition.
Kloiber, et al., (2002)	Relative (image-to-image) normalization	SD	Lakes on Twin Cities Metropolitan Area (TCMA) in east – central Minnesota (USA)	Relative (image-to-image) normalization by applying regression models to pseudo invariant ground targets (targets that have stable reflectance over time) to normalize multitemporal

				images to a single reference scene
Olmanson, et al., (2008)	Each image was calibrated individually with field data, not atmospheric correction was performed.	SD and TSI	A 20-year monitoring of 10,000 lakes in Minnesota (USA).	Used Landsat TM and ETM+ data to generate water clarity census of lakes.
Domínguez Gómez, et al., (2009)	Based on Gilabert, et al., (1994) correction where the value of the ozone optical thickness is 0 and the transmittance due to ozone is 1	Cl a, SD and TSS.	'Parque Regional del Sureste', in Madrid, Spain	Retrieval of algorithms with field measurements of Cl a, SD and TSS.
Matthews, et al., (2010)	DOS and 6S	Chl a, TSS, absorption by CDOM (aCDOM) and SD	Zeekoevlei Lake, a small freshwater lake situated on the Cape Flats, Cape Town (South Africa)	Atmospherically corrected images are evaluated using comparisons with in situ reflectance and Aerosol Optical Thickness (AOT) measurements.
Hicks, et al., (2013)	COST-DOS (Chavez, 1996)	TSS and SD.	34 shallow lakes in the Waikato region, over a 10-year time span (New Zealand)	Once converted to spectral radiance at the sensor aperture, atmospheric correction was automated using COST-DOS method in which the darkest pixel in each band was used as an estimate of path radiance and was subtracted from the top of the atmosphere radiance
Chao Rodríguez, et al., (2014)	Inversion algorithm based on a simplified radiative transfer	Chl a and SD	Lake Arreo (Spain)	With field measurements, an algorithm was fitted for water bodies with similar characteristics of Chlorophyll-a

	model (the ozone optical thickness is 0 and the transmittance due to ozone is 1) (Gilabert, et al., 1994)			concentration and transparency (measured as Secchi disc depth). the models derived from it can be used to detect departures from the expected behavior and, thus, as indicators of environmental stress.
Bernardo, et al., (2017)	Evaluated DOS, QUAC, FLAASH, ACOLITE and L8SR. The best performance was exhibited for L8SR.	TSS	Barra Bonita Hydroelectrical Reservoir located in São Paulo State (Brazil)	An empirical TSS model was developed using in situ measurements and atmospherically corrected images
Ren, et al., (2018)	6S model.	SD	Three Gorges Reservoir on the Yangtze River is the largest hydroelectric project in the world. (China)	In situ SD measurements and spectral data were used to develop the Landsat 8 OLI-based remote retrieval model for SD.
Boucher, et al., (2018)	DOS	Chl a	192 lakes from Maine and New Hampshire (USA)	Explores the relationship between in-lake measured chl and remotely sensed chl a retrieval algorithm output

SD: Secchi Disk

ST: Surface Temperature

Chl a: Chlorophyll a

TSI: trophic-state index

TSS: Total suspended solids

CDOM: Colored dissolved organic matter

Atmospheric models may provide better results, but they are complicated to implement and require input data that are not always available. The most rigorous method of radiometric calibration involves the use of radiative transfer models to produce an absolute correction, while simple radiometric correction techniques such as dark pixel subtraction and Sun angle correction but they are insufficient (Kloiber, et al., 2002).

In 2012, the USGS (United States Geological Survey) Earth Resources Observation and Science Center (EROS) released a global land surface reflectance (SR) coverage from Landsat archived using the atmospheric correction chain LEDAPS (Claverie, et al., 2015; Masek, et al., 2006).

However, maintaining consistent datasets of Surface Reflectance (SR) is an important challenge to ensure long-term quality. Claverie, et al., (2015) analyzed 4000 random Landsat scenes globally distributed from 2000 to 2013 by cross comparison with MODIS SR product data with TM and ETM + spectral responses and the overall results of both approaches show a good match in over 80% of the scenes.

Maiersperger, et al., (2013) evaluated the Landsat SR products by comparisons between aerosol optical thickness derived from AERONET, as well as reflectance correlations with field spectrometer and MODIS data. The results indicated similarity between LEDAPS and alternative data products in longer wavelengths over vegetated areas with no adjacent water, while less reliable performance was observed in shorter wavelengths and sparsely vegetated areas.

2 OBJECTIVES

2.1 General Objective

To assess the use of Landsat TM5 images which have been atmospheric correction with LEDAPS developed by the USGS for studying water quality time series.

2.2 Specific objectives

- To evaluate the Landsat TM 5 atmospherically corrected images by LEDAPS algorithm, using reflectance field data measured in water bodies.
- According to the results, develop an algorithm for the estimation of water transparency as a variable of water quality, that can be applied to a wide variety of lakes and reservoirs, using the Surface Reflectance Landsat TM data product.
- To validate the developed model in different dates, using Secchi Disk field data.
- To inventory the existing water bodies within the natural park “Parque Regional del Sureste” (Madrid) from 1984 to 2011.
- To study the trophic state of these water bodies from 1984 to 2011, based on the OECD classification.
- To assess the ecological status of the mentioned water bodies from 1984 to 2011, according to the objective of the European Water Framework Directive.

3 STUDY AREA

Since 1949, mining activity has been performed in the south part of Madrid Community (Spain), distributed mainly bellow the confluence of the Manzanares and Jarama Rivers (Figure 6).

There were four main types of extractive activities in the area: a) Hillside quarries for extraction of gypsum; b) Hillside quarries for extraction of dry materials; c) Gravel beds above groundwater level; and d) Gravel beds below groundwater level (extensive areas10 hectares and less than 10 meters deep). This activity has resulted in the generation of gravel pit ponds due to outcrop of the phreatic level when the dredging is done. These artificial ponds and lakes, when abandoned, turned into wetland ecosystems with an established aquatic fauna and flora (Domínguez Gómez & Peña, 1999).

In 1994, this zone was declared as a protected area and recognized as “Parque Regional del Sureste” (PRSE) (Official Bulletin of Madrid – BODM 163, July 12th, 1994). The main purpose of the natural park declaration is to protect this area against all kind of negative environmental impact, having as a result the monitoring and control measures of gravel extraction.

The natural park has an extension of 300 Km^2, belonging to 18 municipalities (Figure 7): Torrejón de Ardoz, San Fernando de Henares, Coslada, Mejorada del Campo, Velilla de San Antonio, Rivas-Vaciamadrid, Arganda, Madrid, Getafe, Pinto, San Martín de la Vega, Valdemoro, Titulcia, Ciempozuelos, Chinchón and Aranjuez (Roblas Moreno & García-Avilés, 1997).

In 1997, the first inventory of water bodies defined 123 wetlands within the PRSE: 115 wetlands as a result of human activity (111 of mining extraction, 2 dams, 1 irrigation reservoir and 1 well) and 8 of natural origin (Figure 8). The total area occupied by water bodies within the Park is 411.1 hectares. The size of the ecosystems studied is highly heterogeneous, having wetlands that occupy a few square meters, to some gravel ponds that reach areas of several tens of hectares (Roblas Moreno & García-Avilés, 1997). 96 of total wetlands are located in the Jarama basin, 11 wetlands in Henares basin and 16 in Manzanares basin.

The 2nd Inventory of water bodies was carried out by “Centro de estudios y experimentación de obras públicas (CEDEX)” in 2002, where has been made the thematic map of 103

identified wetlands with Chlorophyll a, transparency (Secchi disk), suspended solids and temperature information.

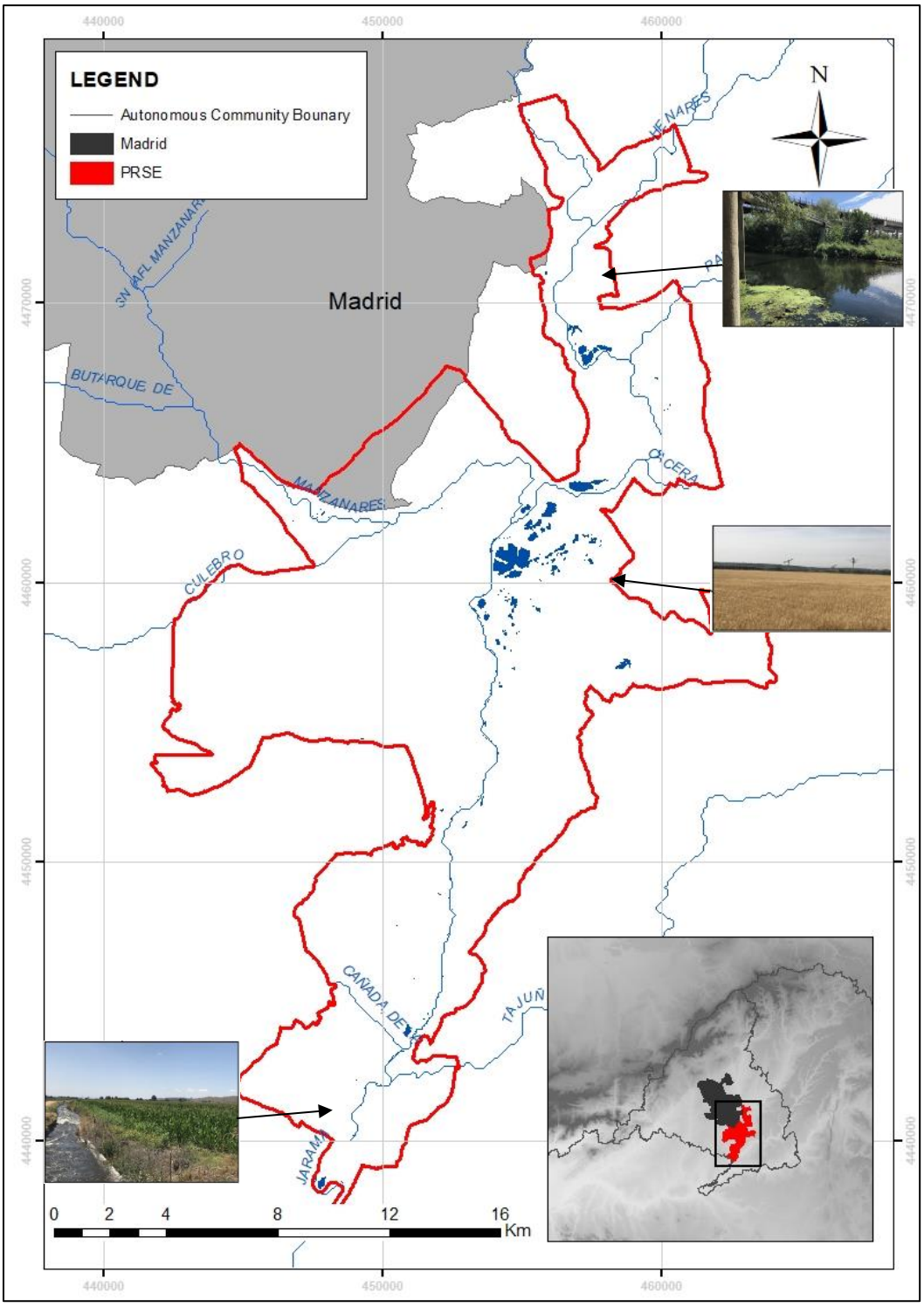

Figure 6. Study area location.

Table 3. Municipalities in the PRSE

Municipality	No. of wetlands	% of Wetlands	Area (Ha)	% area/total wetlands
San Fernando de Henares	6	4,88	4,81	1,17
Velilla de San Antonio	14	11,38	66,05	16,07
Mejorada del Campo	5	4,07	4,19	1,02
Rivas-Vaciamadrid	28	22,76	171,22	41,65
Arganda	17	13,82	41,73	10,15
San Martín de la Vega	29	23,58	90,83	22,09
Ciempozuelos	11	8,94	15,16	3,69
Getafe	11	8,94	5,11	1,24
Aranjuez	1	0,81	12	2,92
Madrid	1	0,81	0,0004	
Total	**123**		**411,13**	

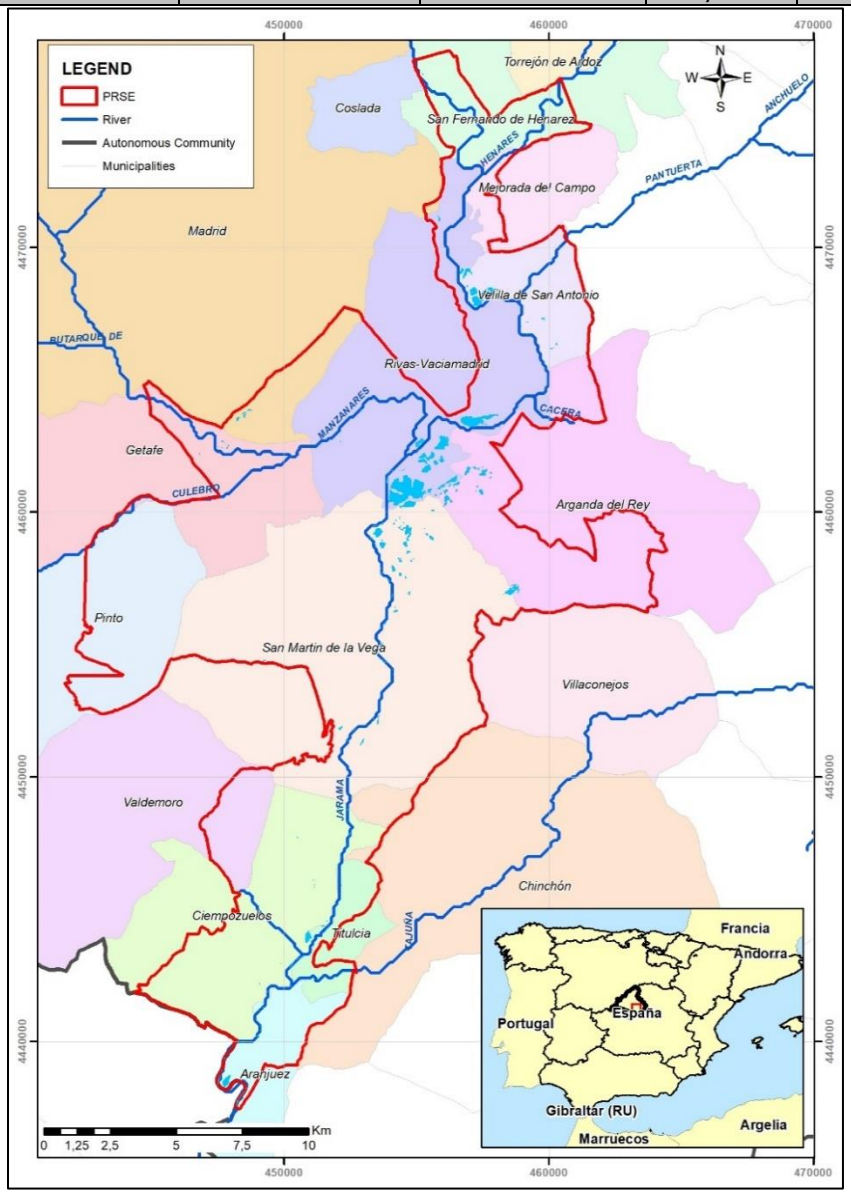

Figure 7. Municipalities in the Natural Park

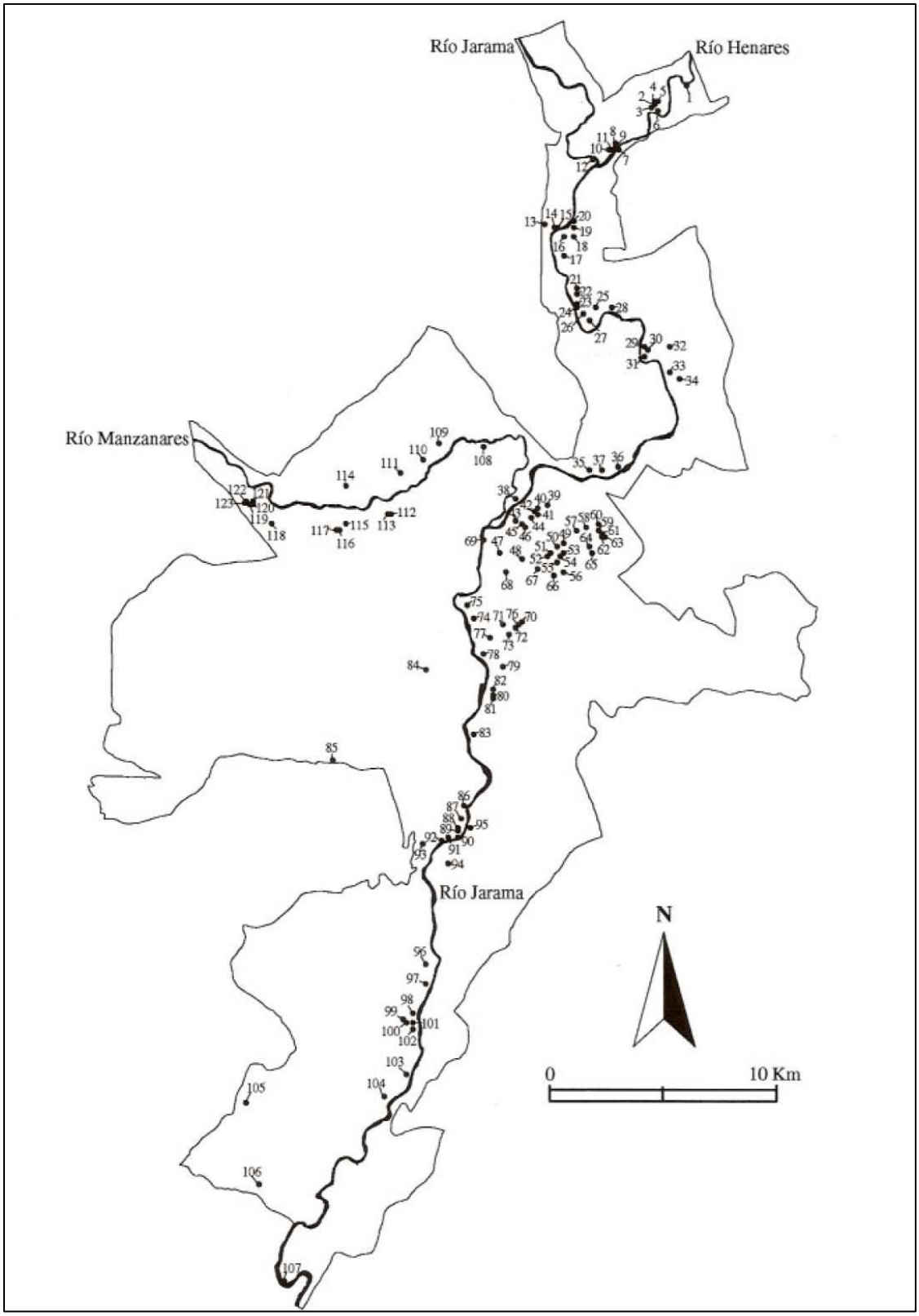

Figure 8. Wetlands location. (Roblas Moreno & García-Avilés, 1997)

3.1 Physical Environment

Geologically, the natural park is characterized by the presence of two fundamental lithological domains: The Neogene Tertiary and the Quaternary. The Neogene Tertiary made up of carbonates and gypsum associated with depositional regimes of alluvial systems. Throughout the Quaternary was developed deposits mainly of fluvial, eluvial and colluvium sediments and a large number of terraces in a repetitive sequence (Figure 9) (Roblas Moreno & García-Avilés, 1997; Mostaza-Colado, et al., 2018).

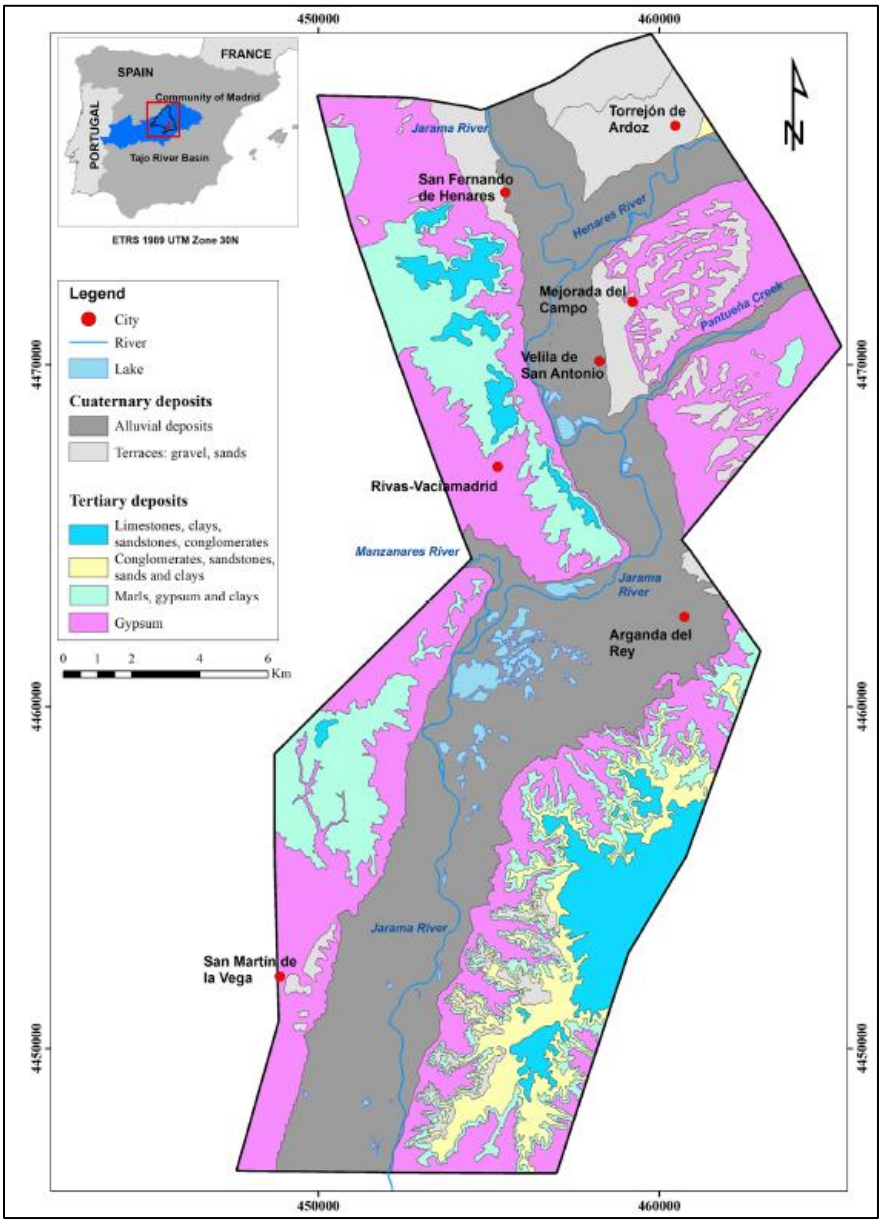

Figure 9. Geological context of the study area (Mostaza-Colado, et al., 2018).

The climate in the study area is considered as Mediterranean temperate-continental, with temperate winters and, warm, dry summers. The average temperature is 13.8 °C, and the average rainfall is 440 mm/year (Mostaza-Colado, et al., 2018).

Hydrologically, the territory under analysis is included in the Tajo basin, specifically in the sub-basin belonging to the Jarama River, which is the main water course of the Park that runs in the North-South direction. In addition to Jarama and Manzanares rivers, the confluences of the Henares and Tajuña rivers with the Jarama river are included. Streams such as Pantueña and Culebro with permanent condition, and others clearly temporary, such as Cacera, Barranco de los Almendros, and Arroyo de la Cañada complete the fluvial network of the Park, at large-scale. The water quality of the main rivers of the Park is poor, as a result of the negative influence exerted by the urban centers (highlighting Madrid) and the industrial activities (Roblas Moreno & García-Avilés, 1997).

3.2 Biological environment

The extraction of aggregates (gravel) activity implies the elimination of the original vegetation cover in the sheets of water. However, as a consequence of the appearance of the pit ponds, a vegetation consisting basically of helophytes was developed, but depending of several factors such as activity, abandonment time, sludge discharge, morphometry of the bucket and degree of entanglement of the sheet of water, among others, reaches a greater or lesser degree of development.

Another important factor is the proximity to the fluvial course. The presence of reed (*Phragmites australis*), accompanied sometimes by bulrush (*Typha spp*.) and junqueras (*Scirpus holoschoenus*), stands out in the existing helophyte vegetation. In zones with a less degraded environment can be found mixed arboreal and taraya groves, although very altered. Finally, it is common the presence of repopulations with different species both native (alders, poplars, elms, etc.) and exotic (paradise tree, weeping willow) in the restored gravel pits.

In terms of fauna, the most representative are the birds, principally composed by Coot (*Fulica atra*), Moorhen (*Gallinula chloropus*), crested grebes (*Policeps cristatus*), small grebes (*Tachybaptus ruficollis*) and mallard (*Anas platyrhyn-chos*). During winter, birds use wetlands as wintering, resting and feeding area.

The fish fauna is the most limited, but it is possible to find 16 species such as boga (*Chondrostoma polylepis*), common barbel (*Barbus bocagei*), rainbow trout, black-bass (*Micropterus salmoides*), pike (*Exos lucius*) and bullhead (*Silurus glanis*). Finally, 10 species of amphibians and 12 reptiles, including the Spanish pond turtle (*Mauremys leprosa*), a specie classified as vulnerable in the Regional Catalog of Endangered Species (CAM), is reported in the study area (Asociación Ecologista del jarama "El Soto", 2001).

3.3 Trophic state

The trophic state of the gravel pit ponds depends of human intervention level (Alvarez Cobelas, et al., 2000):

- During the exploitation - It has a high degree of deterioration due to the contribution of nutrients. For example, El Porcal pond is Hypertrophic.
- The operation has been completed and the gravel pit pond has been abandoned, which is the case of El Campillo pond in eutrophic state.
- Recovered and under a conservation plan, such as Las Madres pond in oligotrophic state.

In 2000 a physic-chemical study of the different types of lentic environment of the park was done (Alvarez Cobelas, et al., 2000). Given the huge number of water bodies existing in the area, a selection of 18 of them has taken place in order to characterize all the variability. The result presents that the majority of water bodies are classified in Hypereutrophic state with 36%, followed by Eutrophic and Mesotrophic state with 29%, and Oligotrophic with 6% (Figure 10):

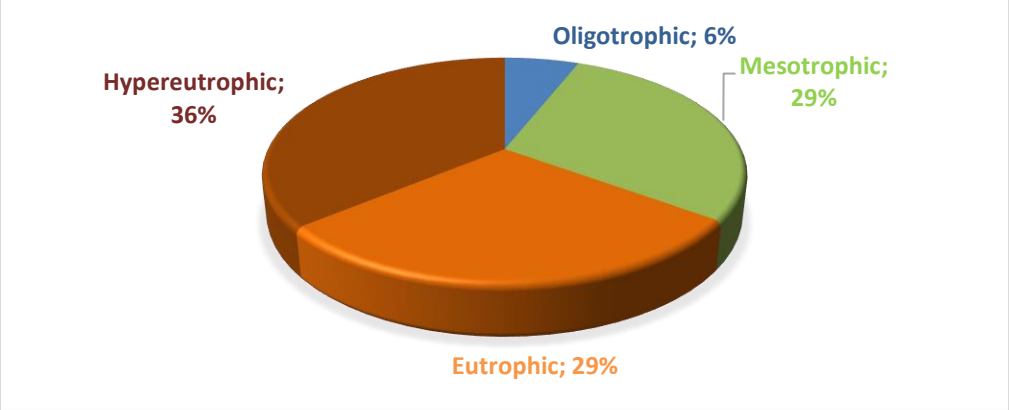

Figure 10. Classification according to the trophic state of the studied ponds. Adapted from Álvarez Cobelas, et al. (2000).

In 2002, on the 2nd Inventory of water bodies carried out by CEDEX , the classification of trophic state has been developed, with 49% of water lakes classified in Oligotrophic state, 26% in Mesotrophic state, 11% in Eutrophic state, 10% in Hypereutrophic state and 4% in Oligotrophic (Figure 11).

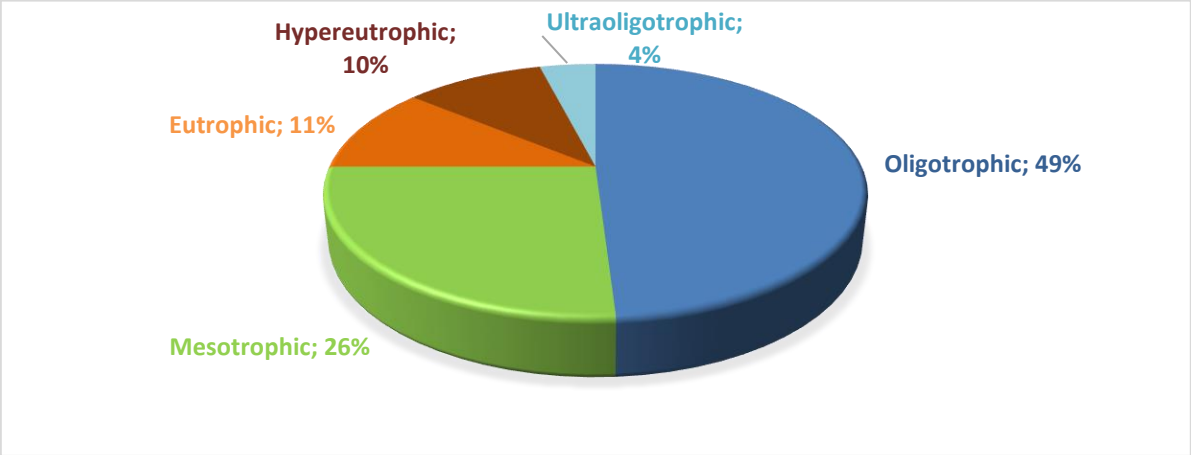

Figure 11. Classification according to the trophic state of the studied ponds. Adapted from CEDEX (2002).

Accordingly, a different situation of the lakes is described. In 2002 the quality of water has been reversed, the most abundant water bodies are classified in oligotrophic state and the minority ones in a hypertrophic state.

First of all, the outcomes are dissimilar given that have been developed in different dates. For the other hand, the study in 2000 has taken into account 18 water bodies and it has been carried out by physic-chemical sample, while the study developed in 2002 has considered all water bodies existing in the PRSE and has been carried out by combination of remote sensing and physic-chemical sample.

3.4 Ecological state

Domínguez Gómez, et al., (2009) studied the EQR, defined in the WFD to measure the ecological state of waters, using transparency as parameter through remote sensing. The EQR transparency map is the mean of all the maps as it represents the annual mean (Figure 12):

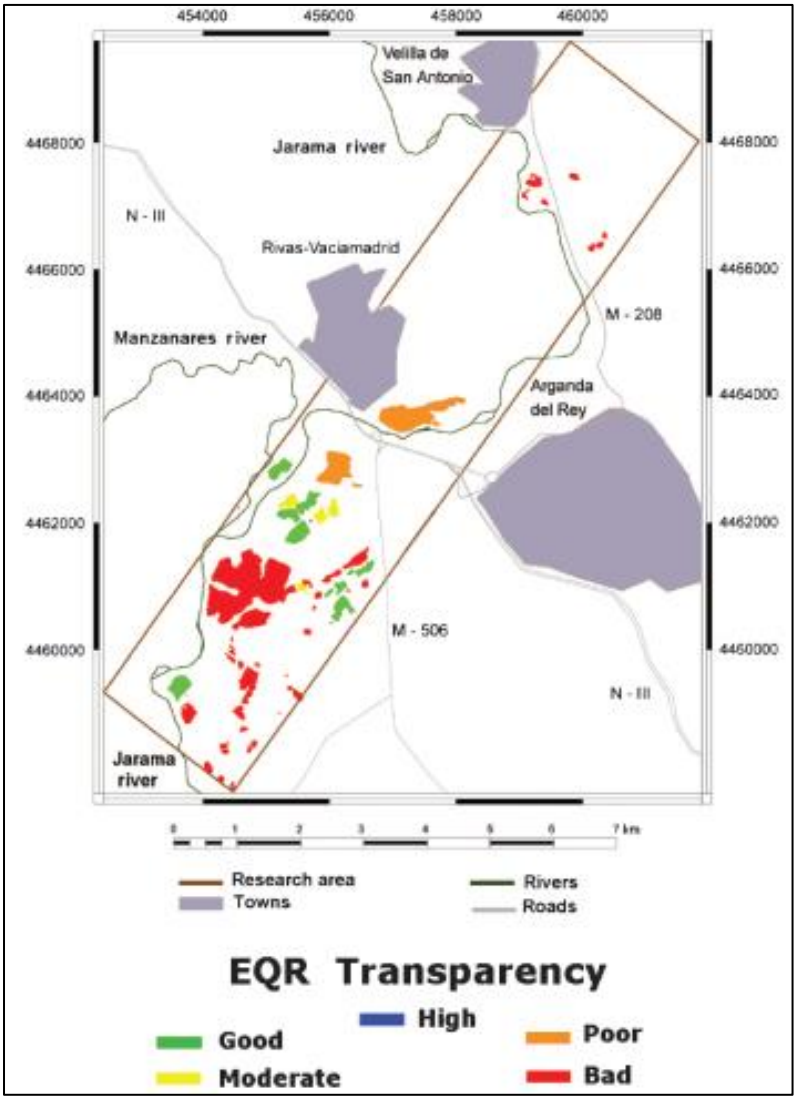

Figure 12. EQR transparency map (Domínguez Gómez, et al., 2009).

4 METHODOLOGY

In this chapter, the methodology followed in this investigation work is presented (Figure 13). First, the surface reflectance images nearest in the time to data measured in the field (Secchi disk and water spectral reflectance), were downloaded from the USGS website, and visually verified to dismiss clouds, shadows or any kind of errors over the study area. Next, the downloaded images were compared with available water spectral reflectance.

According to the results, if the evaluation shows the data are statistically correlated, the Secchi disk (SD) model developed by Domínguez, (2002) can be applied, given that the water reflectance measurements agree with the SD field data and the water reflectance measured in the image bands. Otherwise, a new regression equation with the SD in situ measurements and reflectance measured in the sensor bands must be retrieved and validated.

Moreover, to distinguish water and non-water information, has been assessed three approaches: The Normalized difference water index (NDWI), the Modified Difference Water Index (MNDWI) and the histogram thresholding method. The most accurate method is NDWI and applied to every available image from Landsat5-TM images archive of the area under consideration (scene Path 201 and Row 32) from years 1984 to 2011.

Then, the Secchi disk (SD) model is applied to every image providing a value for each pixel of the SD. Once the SD has been obtained for each image from 1984 to 2011, the Inventory of water bodies in the natural park is carried out, as well as the identification of its trophic state based on the OECD classification and the monitoring of the ecological status of the water bodies according to the European Water Framework Directive.

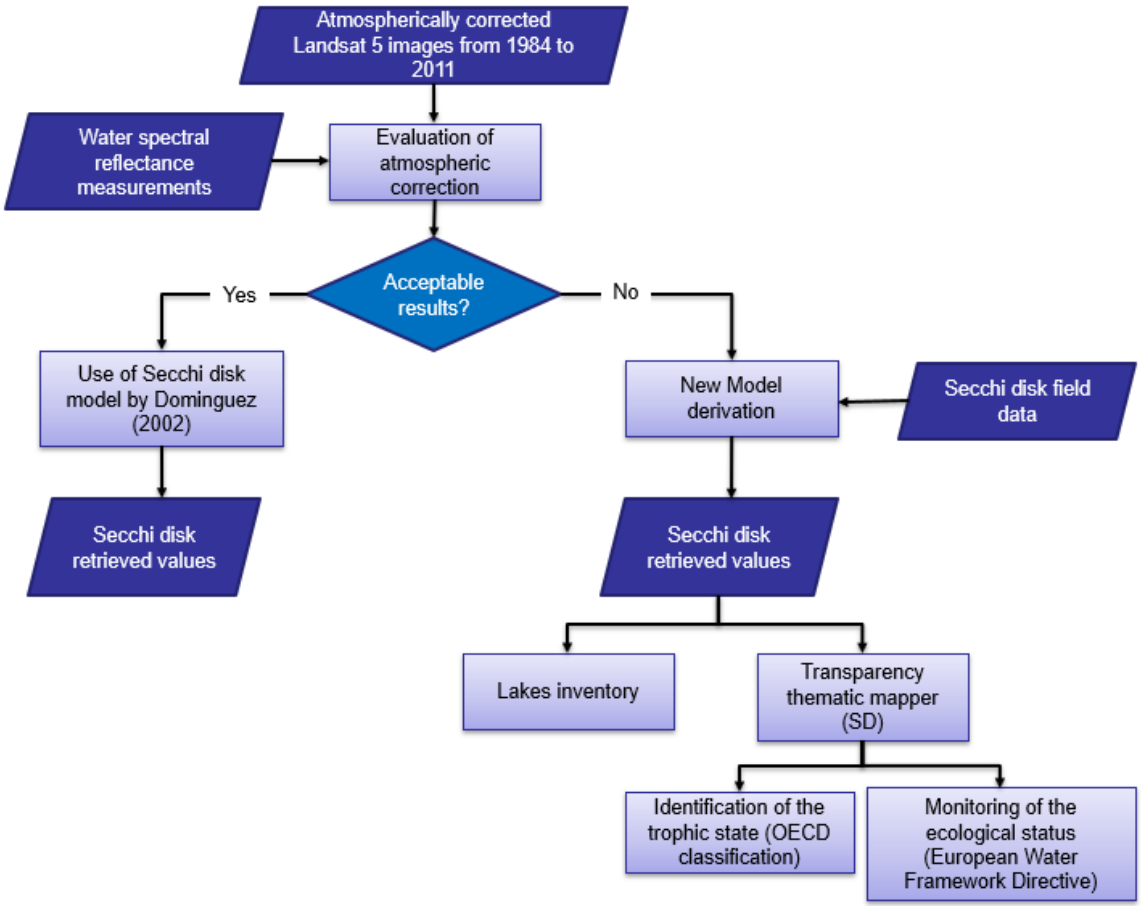

Figure 13. Methodology diagram.

4.1 Data

4.1.1 Landsat 5 images

Landsat satellite data have been produced, archived, and distributed by the U.S. Geological Survey (USGS) since 1972. In compliance with guidelines established through the Global Climate Observing System, USGS has embarked on production of Landsat Science Products to support land surface change studies. Among others terrestrial variables, surface reflectance was derived as data collections suited for monitoring, assessing, and predicting land surface change over time (Masek, et al., 2006).

The Surface Reflectance data product is generated from specialized software called Landsat Ecosystem Disturbance Adaptive Processing System (LEDAPS)[3]. LEDAPS applies atmospheric correction routines to Level-1 Landsat Thematic Mapper (TM) or Enhanced

[3] LEDAPS was originally developed by NASA and the University of Maryland (Masek et al., 2006).

Thematic Mapper Plus (ETM+) data. The algorithm relies on: (i) auxiliary data sources of water vapor, ozone, geopotential height, aerosol optical thickness, and digital elevation (ii) the Second Simulation of a Satellite Signal in the Solar Spectrum (6S) radiative transfer models, (iii) internal aerosol optical thickness (AOT) retrieval; to generate Top of Atmosphere (TOA) Reflectance, Surface Reflectance, TOA Brightness Temperature, and masks for clouds, cloud shadows, adjacent clouds, land, and water (Masek, et al., 2006).

Landsat 4-7 Surface Reflectance data products are available through EarthExplorer[4], under the “Data Sets” > “Landsat” tab for “Landsat Collection 1 Level-2 (On-Demand)”.

Once the order has been submitted and completed, the scenes can be downloaded using the bulk-downloader tool which utilizes Python scripts for data downloads, and it is available on a GitHub repository[5].

The Landsat Surface Reflectance data product is generated at 30-meter spatial resolution on a Universal Transverse Mercator (UTM) and the default file format is GeoTIFF. The data type is 16-bit signed integer, the range is -2000 – 16000, with a valid range of 0-10000 and a scale factor of 0.0001 for all bands.

Landsat5-TM images archive contains a large number of satellite images of the area under consideration (scene Path 201 and Row 32) from years 1984 to 2011. From this historical series, many images with clouds were discarded. Finally, only 230 Landsat 5 scenes were selected for this study (Figure 14).

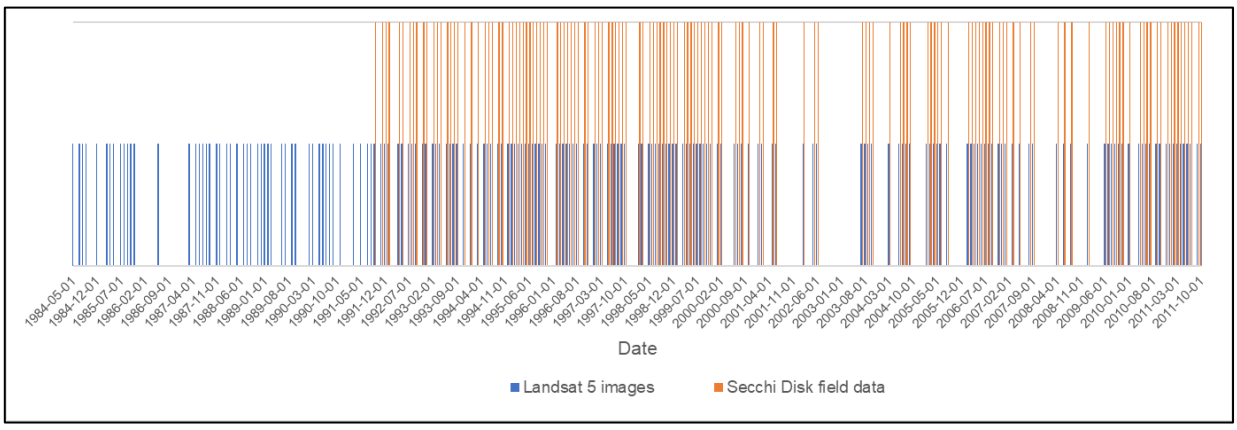

Figure 14. Temporal distribution of Landsat 5 images and field data

[4] https://earthexplorer.usgs.gov
[5] https://github.com/USGS-EROS/espa-bulk-downloader

4.1.2 Reflectance Field data

The water reflectance measurements were carried out with a FieldSpec FR ASD spectroradiometer measured outside of water body in 38 points, during thesis work developed the by Domínguez (2002). The results are shown as water reflectance in percentage (%) in function of wavelength between 350 and 1000 nm.

The continued reflectance values are transformed into discrete values, in order to compare them with the pixel values from the Landsat Surface Reflectance images. For this purpose, the reflectance values for a given band are calculated as (NASA, 2001):

$$L_{\lambda\,(b,s)} = \frac{\int RSR(b,\lambda) L_{\lambda\,(s,\lambda)} d\lambda}{\int RSR(b,\lambda) d\lambda} \quad (3)$$

Where:

$RSR(b,\lambda)$ *is the Relative Spectral Response for band "b" at "λ" calculated from component level transmission, reflectance and responsivity measurements.*

$L_{\lambda\,(s,\lambda)}$ *is the measured spectral radiance of sphere level ·s" at "λ.*

4.1.3 Secchi Disk field data

The water transparency expresses by the Secchi Disk depth is measured by means of a white and black disk with diameter generally about 30 cm, that is lowered into a water body until it is no longer viewable by an observer (Figure 15).

Figure 15. Secchi disk measurement.
Practice work during development of MSc. Uses and management of water resources in the natural environment.

The Secchi disk values were obtained from different sources:

- SD measurements carried out on August 13th, 1992 in 16 points on Las Madres, El Campillo and El Porcal ponds (Dominguez Gòmez, et al., 1997) .
- SD data collection of 18 points in October 29th, 1997 in El Campillo and El Porcal ponds (Domínguez Gómez & Peña, 1999).
- Measurements carried out during the thesis work developed the by Domínguez (2002): As the reflectance, the Secchi disk was measured in 38 points in July 3rd and 4th, and 13 in July 31st in Las Madres, El Campillo y El Porcal ponds (Figure 16).
- Measurements carried out by Miguel Alvarez Cobelas[6] from September 1991 to December 2013 in the buoy located in Las Madres pond.
- The 2nd Inventory of water bodies of Parque del Sureste carried out by "Centro de estudios y experimentación de obras públicas (CEDEX)" in 2002, where the research and development of the cartographic representation of the trophic state on wetlands within the PRSE was done. In this research has been made a thematic map of 103 identified wetlands with Chlorophyll a, transparency (Secchi disk), suspended solids and temperature information.

[6] Centro de Investigaciones Ambientales de la Comunidad de Madrid "Fernando González Bernáldez". Available on http://www.humedalesibericos.com/

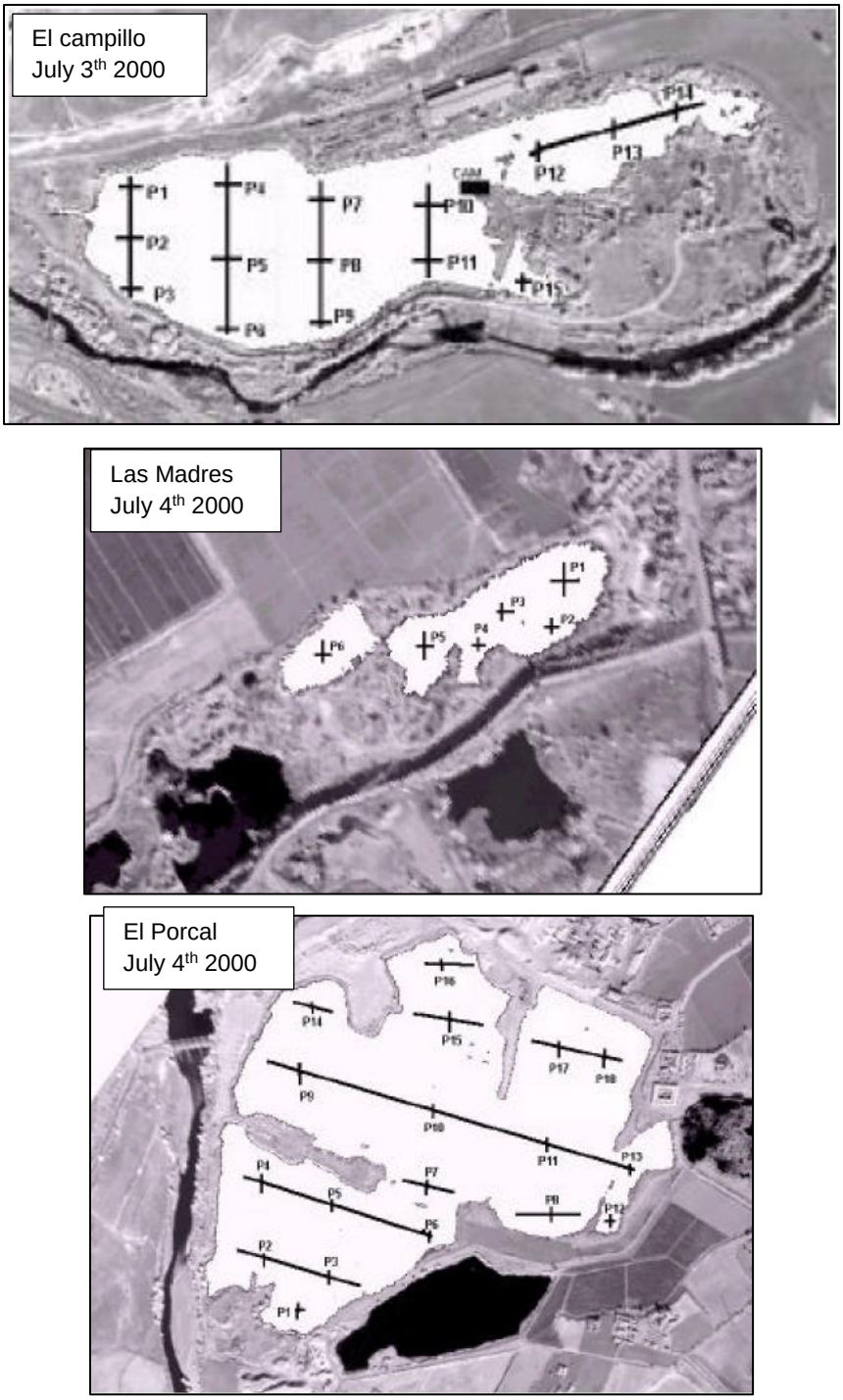

Figure 16. Measurement points of Domínguez (2002)

4.2 Water/land pixel discrimination

Detecting water bodies and accurately delineating it from the surrounding, is the first and important step for monitoring the pit ponds. The traditional methods of visiting the actual site and using survey techniques are time consuming and difficult to implement. Remotely

sensed data, Landsat 5 in particular, provides a functional means to delineate water boundaries over a large area at a specific point in time. With the multiple bands in Landsat 5it is important to understand how to use the image and which spectral band and classification method(s) to use for the best hydrological classification.

Various methods are currently in use for water body extraction, to distinguish water and non-water information by analyzing and discerning spectral features. Among the most common approaches, in the current study the Normalized difference water index (NDWI), the Modified Difference Water Index (MNDWI) and a histogram thresholding method were considered appropriate, to compare accuracy of the results in water bodies detection.

NDWI was initially practiced by McFeeters (1996) to compute water dimensions for wetland environments. Resulting values of NDWI represent that areas covered with water have positive values; however, areas with vegetation or soil tend to have zero or negative values (McFeeters, 1996).

$$\mathrm{NDWI} = \frac{Band\ 2 - Band\ 4}{Band\ 2\ +\ Band\ 4} \qquad (4)$$

Later version of NDWI is called MNDWI generated by Xu (2006). Water features were given in positive values as two classes (water and non-water features).

$$\mathrm{MNDWI} = \frac{Band\ 2 - Band\ 5}{Band\ 2\ +\ Band\ 5} \qquad (5)$$

Then, terrestrial features were masked out to create a water-only image. Finally, the areas belonging to river and mountain zones were also discarded, given that the water bodies under consideration are located only in the flat area.

4.3 Comparison of Landsat 5 Surface Reflectance data product and Reflectance Field data

In order to assess the suitability of the Landsat surface reflectance images corrected with LEDAPS software by the USGS, for water quality studies, the comparison between the reflectance values measured in field (*epigraph 4.1.1*) and the water reflectance measured in the sensor bands (*epigraph 4.1.2*) has been done.

In this study, because the *in situ* measurements were mostly from nearshore complex waters where the water depth and bottom benthic type may change drastically over a very short distance, the satellite surface reflectance from the center pixel (i.e., 1×1) of the Landsat

images closest to an in situ site was used for subsequent analysis, rather the conventional average of a 3×3 pixel neighborhood box (Wei, et al., 2018).

Several metrics were adopted to evaluate the matchups, including the relative root-mean square deviation (rRMSD), bias and mean absolute percentage error (MAPE), expressed as (Wei, et al., 2018):

$$rRMSD = \sqrt{\frac{1}{N}\sum_{i=1}^{N}\left(\frac{S_{i,1} - S_{i,2}}{S_{i,2}}\right)^2} \times 100\% \quad (6)$$

$$bias = median\left\{\left(S_{i,1} - S_{i,2}\right)/S_{i,2} \times 100\%\right\} \quad (7)$$

$$MAPE = \frac{1}{N}\sum_{i=1}^{N}\left|\frac{S_{i,1} - S_{i,2}}{S_{i,2}}\right| \times 100\% \quad (8)$$

Where $S_{i,1}$ and $S_{i,2}$refer to the satellite products and in situ measurements under investigation, respectively, and N the number of data pairs.

The cosine distance was derived to quantify the spectral similarity between satellite and in situ reflectance surface spectra (Wei, et al., 2016):

$$\cos\alpha = \sum_{i=1}^{N}\frac{\left[S_{i,1}.S_{i,2}\right]}{\sqrt{\sum_{i=1}^{N}{S_{i,1}}^2\sum_{i=1}^{N}{S_{i,2}}^2}} \quad (9)$$

where α is the angle formed between the spectra $S_{i,1}$and $S_{i,2}$.

4.4 Developing of SD model using Landsat Surface Reflectance data product

The empirical methodology to obtain the algorithm requires in situ measurements of the Secchi disk, which serve as a basis for establishing an empirical relationship with the water reflectance measured in one or multiple sensor bands. In this case, the number of field sites was determined using common statistical sampling strategies (Domínguez Gómez, et al., 2009):

$$N = \left(\frac{z_c\sigma}{\varepsilon}\right)^2 \quad (10)$$

$$N = \left(\frac{1.96 \times 3}{1}\right)^2 = 34.5744 \quad (11)$$

Where

N is the number of samples.
z_c the confidence coefficient (z_c = 1.96 for a confidence interval of 95%).
ε the error of estimation (1 cm according to Domínguez Gómez, et al., (2009)).
σ the estimated variance (3 cm estimated by Domínguez Gómez, et al., (2009) from analysis of a long SD measurement series in different reservoirs).

Thus, the number of samples to be used to fit the model had to be > 35. On the other hand, the analysis of the diffuse attenuation coefficient (Kd) for each band allows to choose the band between 520nm and 600nm (green band) because it is the one with a smaller Kd and consequently with the highest light penetration (Domínguez Gómez, et al., 2009).

4.5 Model Validation

Assessing accuracy of obtained remote sensing Secchi Disk requires in situ measurements contemporary to image acquisition, since lake conditions may change rapidly. Retrieved Secchi disk values are compared with measured Secchi disk values (epigraph 5.1.3), different to those used to the model derivation.

Several metrics were used to perform statistical analysis in this study, which include the determination coefficient (R^2), the root-mean-square error (RMSE), and the mean absolute percentage error (MAPE) (Cao, et al., 2018):

$$MAPE = \frac{1}{N}\sum_{i=1}^{N}\left|\frac{\mathrm{SD}_{measured,i} - \mathrm{SD}_{derived,i}}{\mathrm{SD}_{measured,i}}\right| \times 100\% \quad (12)$$

$$RMSE = \sqrt{\frac{1}{N}\sum_{i=1}^{N}\left(\mathrm{SD}_{measured,i} - \mathrm{SD}_{derived,i}\right)^2} \quad (13)$$

Where:

N *is the number of samples,*

$SD_{measured,i}$ *and* $SD_{derived,i}$ *refer to the measured and derived SD values for the* i-*th sample, respectively.*

R^2 presents the correlation degree of the coupled data in the modeling, and the RMSE reflects the difference between the predicted values and the true values (measured); smaller RMSEs indicate higher evaluation accuracies. The MAPE is a measure of the prediction accuracy of a forecasting method; it usually expresses accuracy as a percentage, where smaller MAPEs indicate better modeling results (Cao, et al., 2018).

Once validated, the regression equation is then applied to every image providing a value for each pixel of the Secchi Disk. To apply the regression equation a python language script was developed to automate image preparation and water transparency analysis.

4.6 Inventory of water bodies in the natural park (1984 to 2011).

Once the water/land pixel discrimination using the NDWI for each Landsat 5 scene has been done, it is obtained water mask map and the segmentation of the water mask is done giving one identifier to each water body. Finally, the number and area of water bodies is computed, and the temporal evolution is analyzed.

Only water bodies with area greater than 1800 m^2, equivalent to 2 pixels, in order to eliminate small terrain shadows and additional errors, has been considered.

4.7 Identification of the trophic state of the water bodies based on the OECD classification

The retrieved Secchi disk from Landsat 5 images (epigraph 4.3) provides values of this parameter for every pit pond from 1984 to 2011. Then, the Secchi disk mean value of each water body was used to compute its annual media and to classify them into a trophic status category.

The OECD method evaluates the probability distribution of five trophic classes: ultra-oligotrophic, oligotrophic, mesotrophic, eutrophic or hypertrophic, considering the mean annual value of SD transparency (epigraph 1.5).

4.8 Monitoring of the ecological status of water bodies according to the WFD

As mentioned in epigraph 1.5, according to the WFD, the ecological state of a waterbody should be defined relative to the annual media value deviation from the reference condition, using the Ecological Quality Ratio (EQR). Given this, the reference ecological value chosen

is SD = 5 m and the EQR categorization for the water bodies was done with the classification (Søndergaard, et al., 2005):

- bad: 0–0.2
- Poor: 0.2–0.4
- moderate: 0.4–0.6
- good: 0.6–0.8
- high: 0.8.

An EQR was calculated for every pond using 27 years of data from 1984 to 2011.

5 RESULTS AND DISCUSSION

5.1 Water/land pixel discrimination

According to the histogram thresholding method based on the Near infrared band, the Landsat 5 scenes were visually analyzed to obtain a threshold, where all pixels with reflectance in band 4 below that threshold correspond to water or shadows. The obtained threshold was 700 (Figure 17).

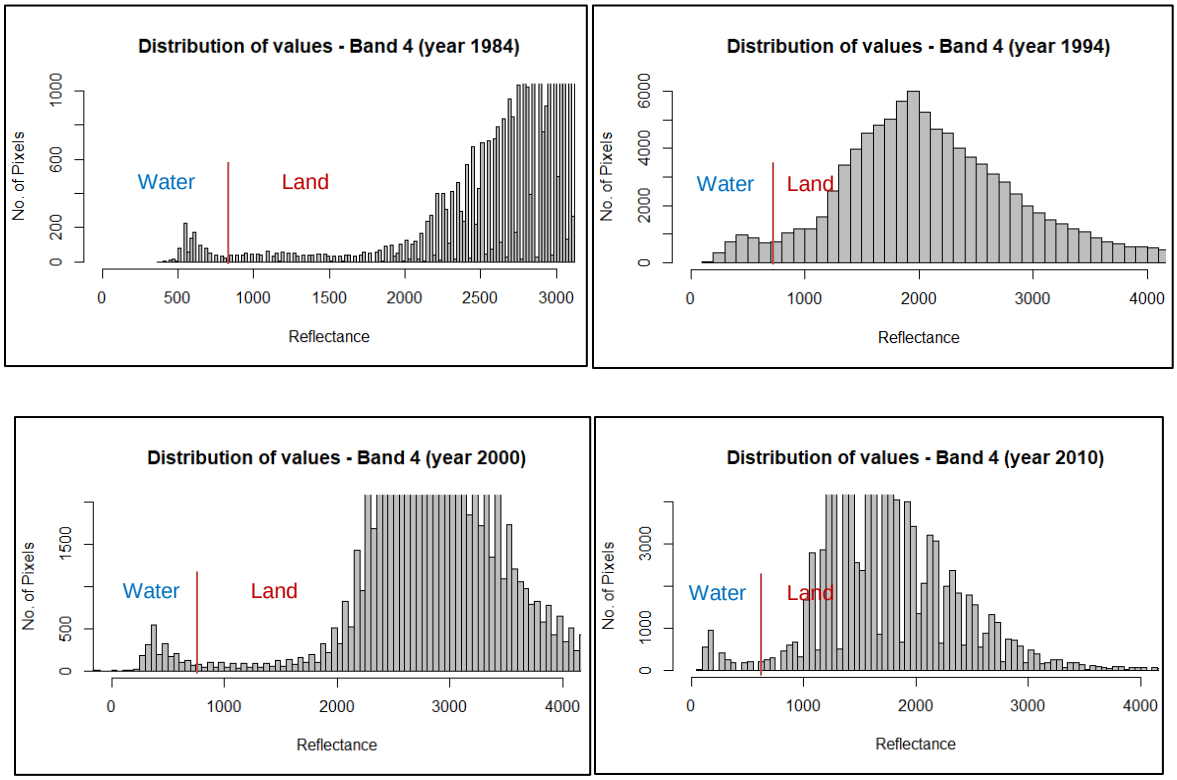

Figure 17. Histogram thresholding method

Once obtained the discriminated water bodies by NDWI, MNDWI and histogram thresholding methods, the accuracy assessment with the available field data was carried out for images belonging to 19-08-1992, 29-10-1997, 11-06-2000, 29-07-2000, by comparison of the obtained water bodies and real data on the field.

In figure 18, it is possible to observe the field data (red marks) located into the classified pit ponds in the case of NDWI (Dark blue) and MNDWI (light blue). The NDWI has the ability of extracting more water body related information, while MNDWI mistakenly extracts some

small shadow and errors in the images, which presents a limitation for the extraction of small water bodies.

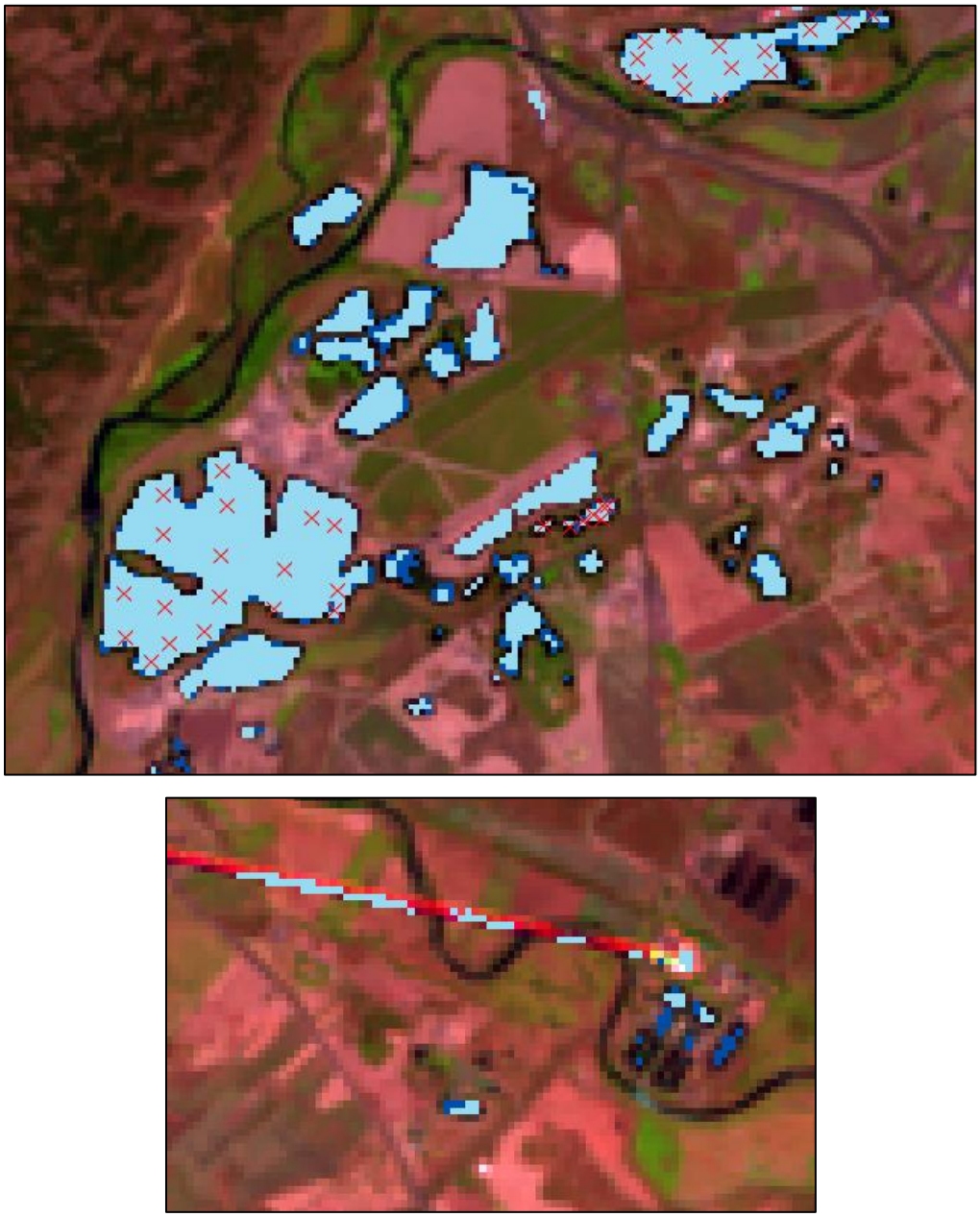

Figure 18. Water discrimination based on NDWI and MNDWI methods. Date: 2000/06/11. Light blue: MNDWI; Dark blue: NDWI. False color background RGB: 543.

Based on the results, NDWI generated more accurate result, so this method was applied in the study. Limitations of the selected method are associated with fact that it relies only on spectral feature analysis; terrain shadows with spectral characteristics extremely similar to

those of water cannot be eliminated completely. In addition, the inherent spatial resolution of the Landsat 5 imagery prevents detection and extraction of very small water bodies (Duru, 2017).

5.2 Comparison of Landsat 5 Surface Reflectance data product and Reflectance Field data

The surface reflectance data products are evaluated with concurrent in situ hyperspectral surface reflectance measurements.

Visual observation indicates qualitative consistence between the Landsat surface reflectance spectra (Figure 19) and in situ data (Figure 20).

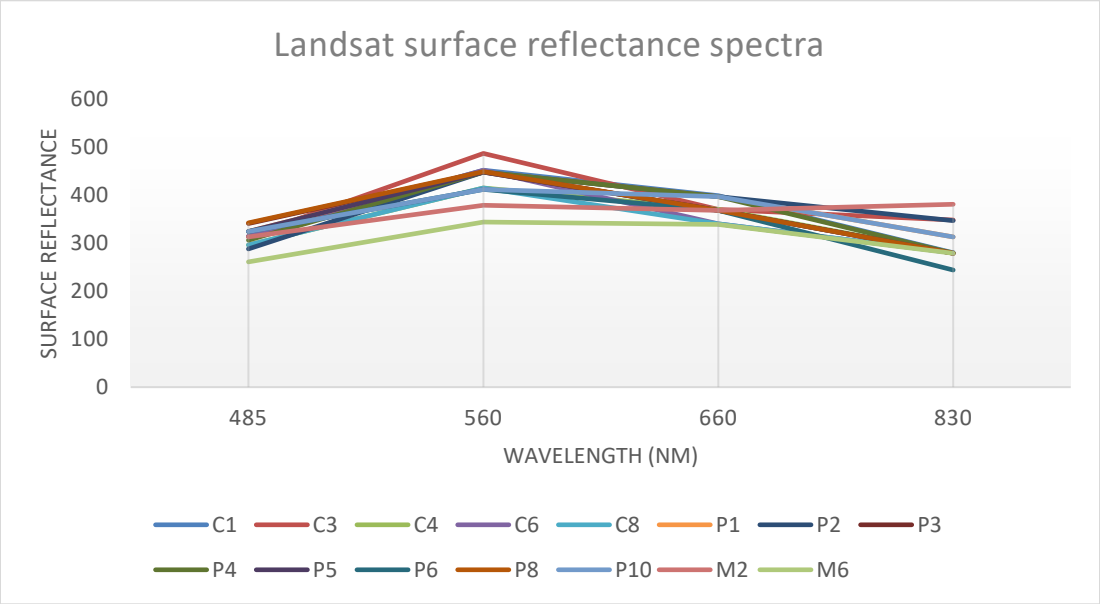

Figure 19. Landsat 5 surface reflectance spectra.

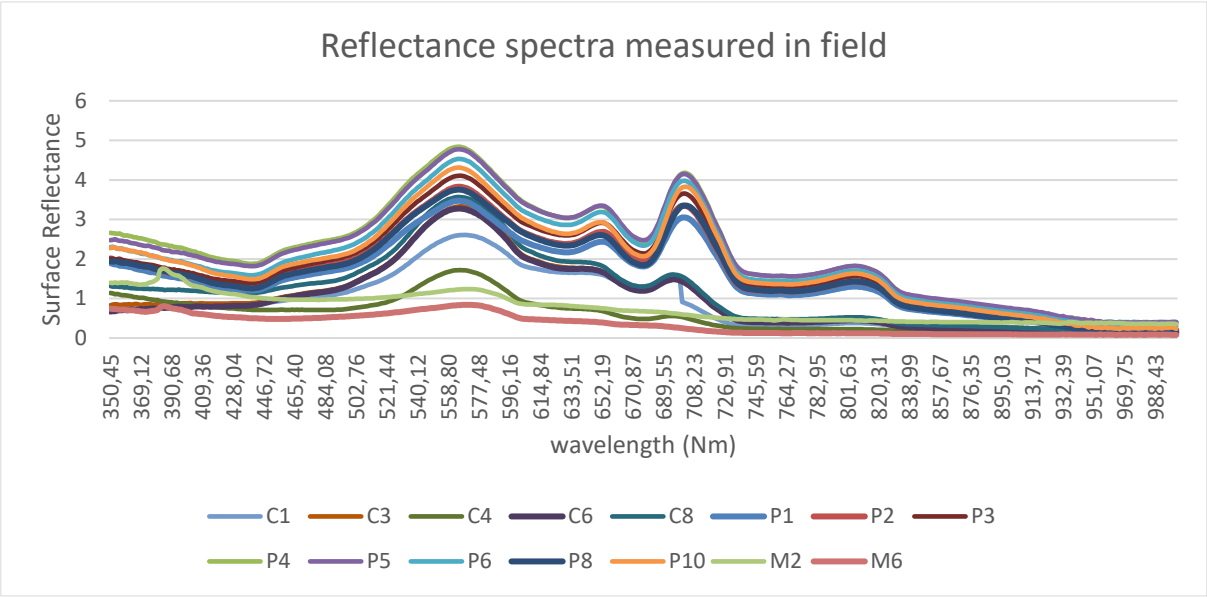

Figure 20. Reflectance spectra measured.

The scatter plots between in situ and satellite matchup surface reflectance are shown in Figure 21. It is visible from the scatter plots that the Landsat 5 Surface reflectance has a large deviation from 1:1 line with a small R^2, due to the significantly overestimated Landsat surface reflectance. In band 4, for example, when the measured reflectance is 0.01, the Landsat surface ranges from 0.04 to 0.05, which means 80% of difference.

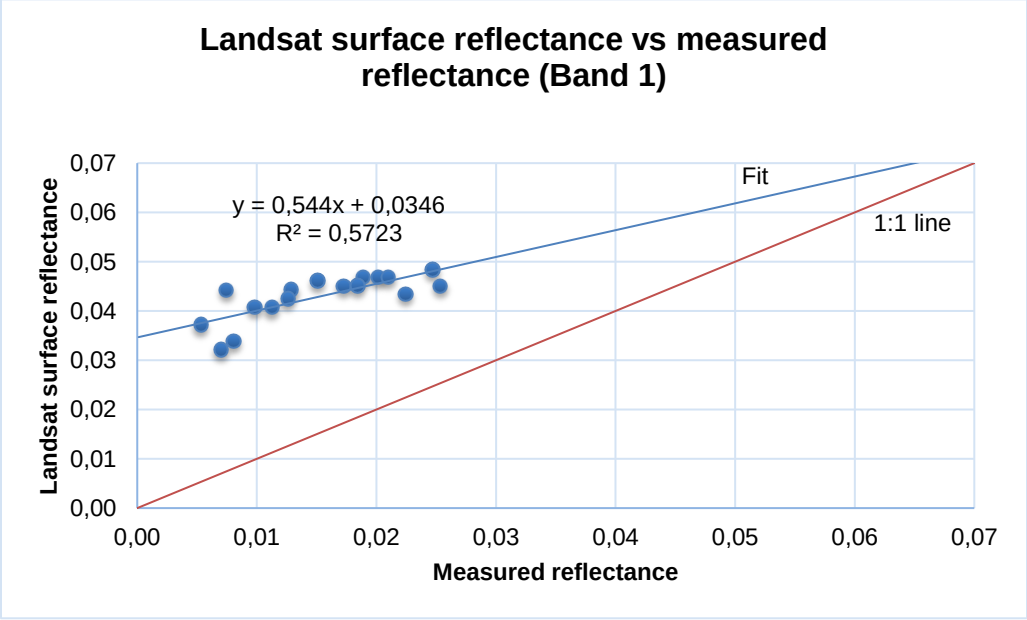

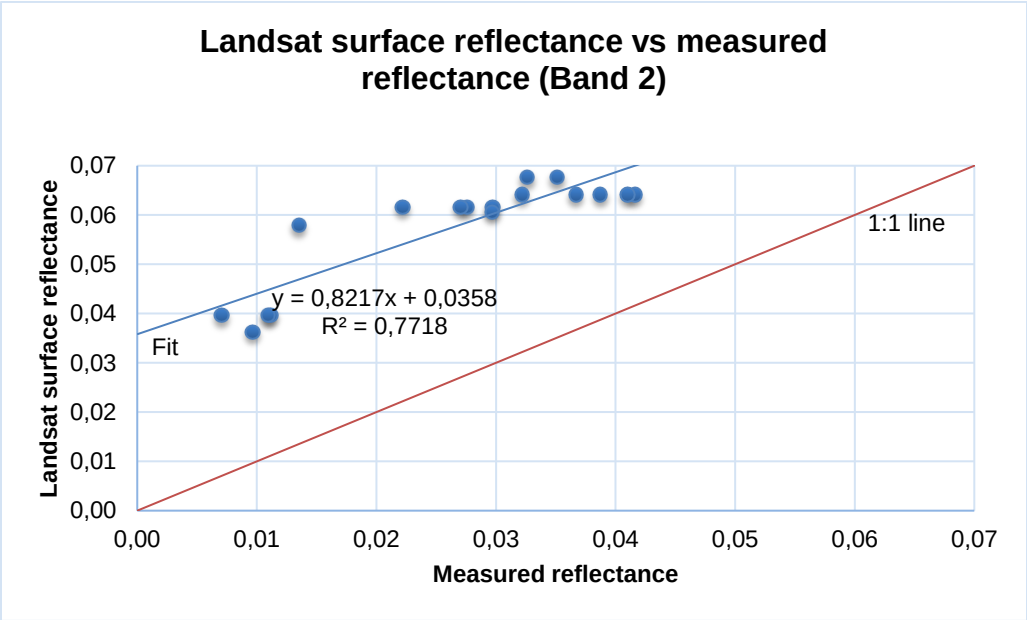
Landsat surface reflectance vs measured reflectance (Band 2)
Landsat surface reflectance
0,07
0,06
0,05
0,04
0,03
0,02
0,01
0,00
y = 0,8217x + 0,0358
R² = 0,7718
Fit
1:1 line
0,00
0,01
0,02
0,03
0,04
0,05
0,06
0,07
Measured reflectance

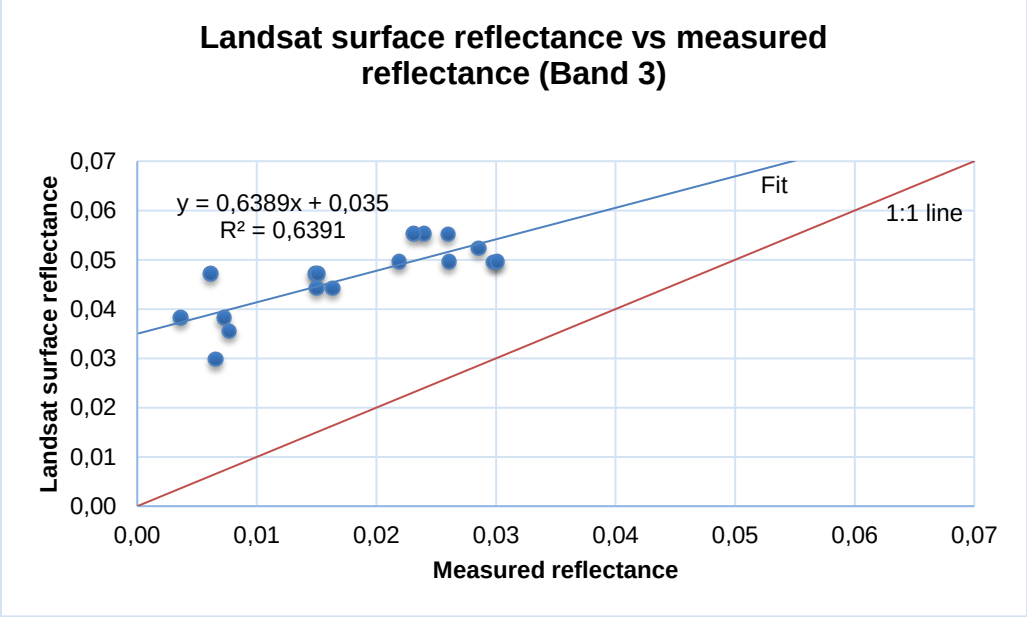
Landsat surface reflectance vs measured reflectance (Band 3)
Landsat surface reflectance
0,07
0,06
0,05
0,04
0,03
0,02
0,01
0,00
y = 0,6389x + 0,035
R² = 0,6391
Fit
1:1 line
0,00
0,01
0,02
0,03
0,04
0,05
0,06
0,07
Measured reflectance

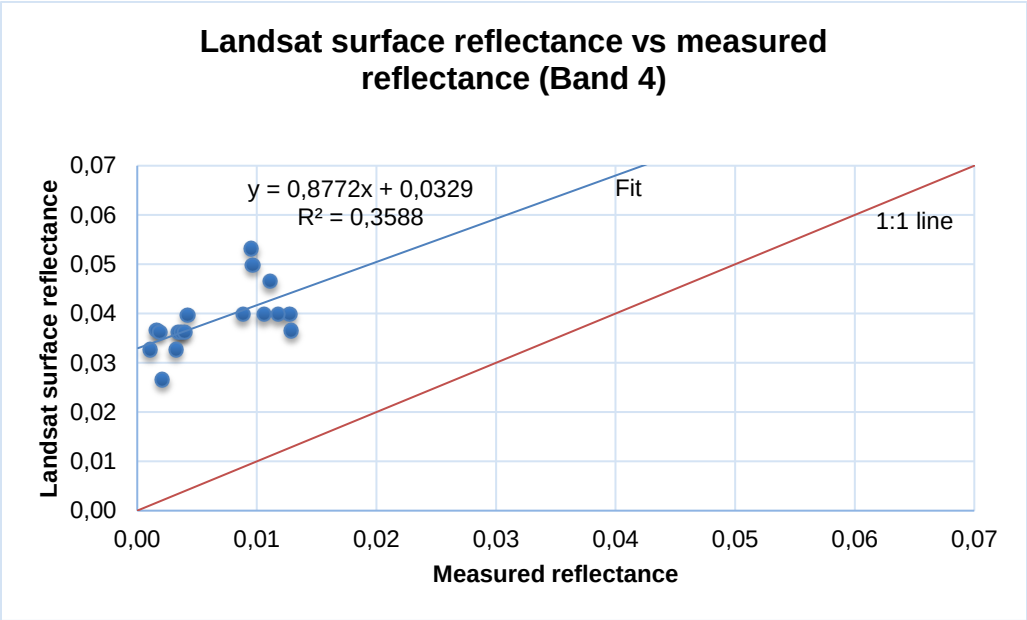

Figure 21. Landsat 5 Surface reflectance versus measured reflectance

According to other criteria including bias, MAPD and rRMSD, it is visible the overall low accuracy where the minimum bias, rRMSD and MAPE values are 107,3, 388,6% and 162,9%, respectively, achieved in band 2. But the cos α have shown similarity between satellite and in situ surface reflectance spectra. Those metrics indicates a poor correlation between measured and Landsat surface reflectance. This result agrees with Maiersperger, et al., (2013), who indicated similarity between LEDAPS and alternative data products in longer wavelengths over vegetated areas with no adjacent water, while less reliable performance was observed in shorter wavelengths and sparsely vegetated areas.

Table 4. Statistical results for the remote sensing reflectance matchup. The best performance is rendered in bold face

Band	Bias (%)	rRMSD (%)	MAPE (%)	cos α
1	205,626	753,563	235,601	0,950
2	**107,388**	**388,629**	**162,932**	**0,966**
3	169,937	1198,396	256,975	0,939
4	812,630	13263,815	877,257	0,883

5.3 Developing of SD model using Landsat Surface Reflectance data product

According to the comparison of Landsat Surface Reflectance data product and Reflectance Field data results, it is not possible to apply the models previously developed for the study area e.g. Domínguez Gómez, et al., (2009). Thus, a total of 40 points has been selected to retrieve the new empirical relationship between the water reflectance measured in the field and the water reflectance measured in the sensor green band.

In Figure 22 is shown the relation between the measured in the field and surface reflectance measured in the atmospherically corrected Landsat 5 image.

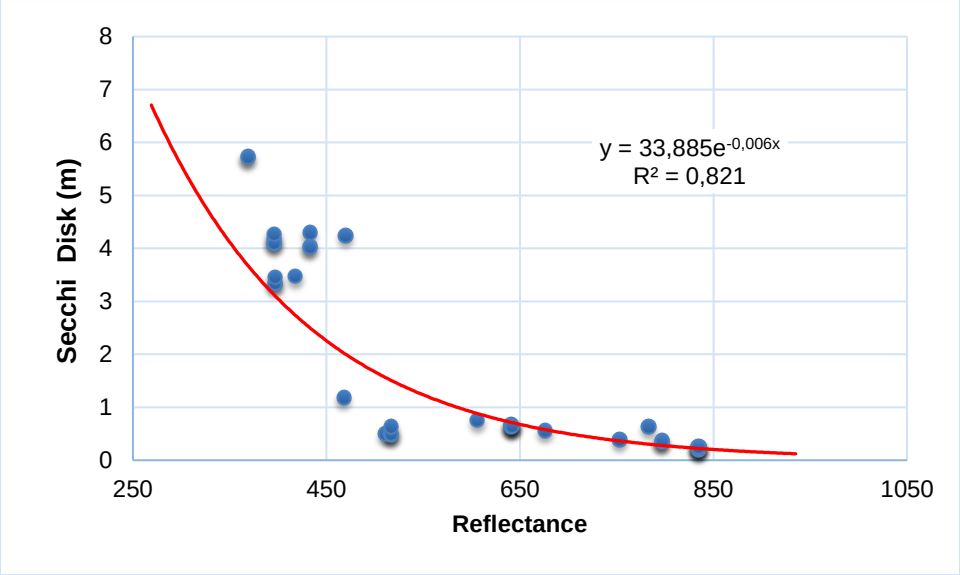

Figure 22. Relation of Secchi Disk and Landsat 5 surface reflectance band 2.

5.4 Model Validation

The obtained algorithm was then applied to the second group of data reserved for testing and results were compared with the Secchi disk field data. The RMSE equal to 0,59 m reflects the difference between the predicted values and the true values (measured); smaller RMSEs indicate higher evaluation accuracies. The MAPE equal to 30,49% is a measure of the prediction accuracy of a forecasting method; it usually expresses accuracy as a percentage, where smaller MAPEs indicate better modeling results.

In Figure 23 is exhibited a small bias from the *in situ* data, with a linear slope close to 1:1 line and R^2=0.68, which presents a good correlation degree of the coupled data in the modeling.

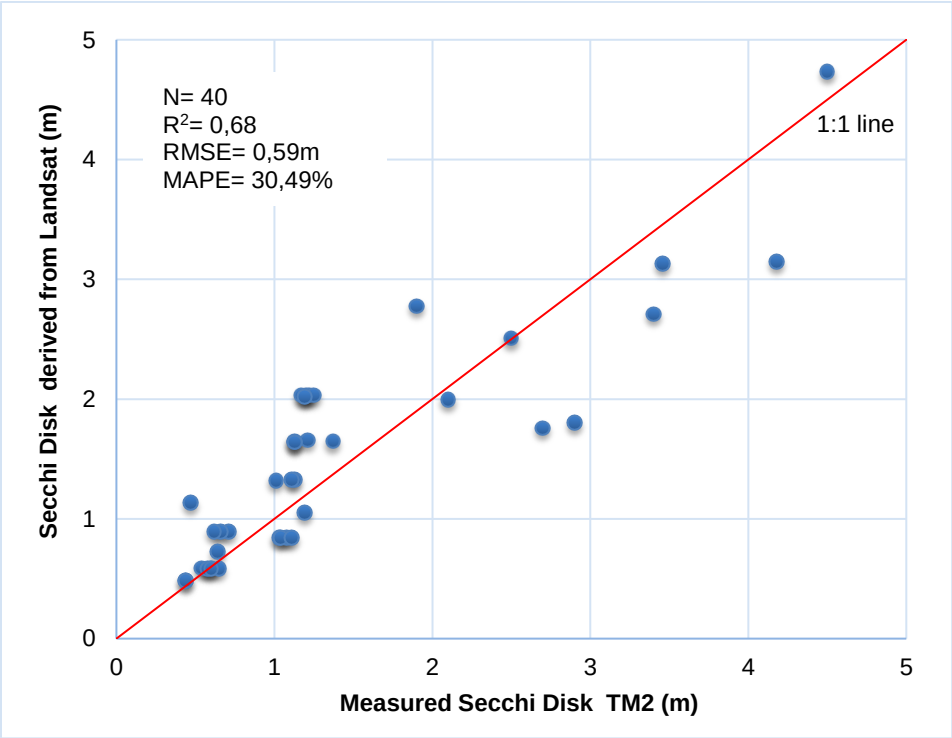

Figure 23. Relation of Secchi Disk and Landsat surface reflectance band 2.

A large number of models to estimate SD from TM reflectance information can be found in the appropriate literature. In table 5 is summarized the statistical analysis of algorithms retrieved by different authors.

Compared with the mentioned authors, the obtained model has a high RMSE given the overestimation of Landsat surface reflectance. Despite of the RMSE, the results exhibit an acceptable correlation between the SD field data and Landsat surface reflectance with R^2 of 0.68.

The fact that several investigators have developed similar relationships between SD and Landsat 5 imagery across a broad geographic range (Italy, USA, South Africa, Spain, China, Brazil, New Zealand according to Table 2) and for such widely varying surface waters (estuaries, reservoirs, and inland lakes) is more than coincidence, it confirms the consistency of the relationship between SD and Landsat 5 data.

Table 5. Statistical analysis of predicted and observed Secchi disk obtained by different authors.

Author	Obtained model	R^2	RMSE (m)
Proposed algorith	$\mathrm{SD} = 33{,}885\mathrm{e}\text{-}0{,}006\mathrm{TM2}$	0.68	0.59
Giardino, et al., (2001)	$SD = 8.01\ \mathrm{TM1}/\mathrm{TM2}^{-8.27}$	0.852	0.45
Olmanson, et al., (2008)	$SD = \exp\left[\left(2.2 \times \frac{TM1}{TM3}\right) - (1.1 \times TM1) - 0.58\right]$	0.83	0.292
Domínguez Gómez, et al., (2009)	$SD = 4.0098\ \mathrm{TM2}^{-1.3659}$	0.8969	0.13
Hicks, et al., (2013)	$Ln(SD) = -2.0298 + 2.7517 \times Ln(TM1/TM3) - 0.6022 \times Ln(TM1)$	0.670	0.33
Doña, et al., (2014)	$SD = TM2^{-1.82}$	0.92	0.30
Chao Rodríguez, et al., (2014)	$SD = -10.281\ \frac{TM2 - TM1}{TM2 + TM1} + 4.5753$	0.63	Non-available
Soria, et al., (2017)	$SD = exp(1{,}52 + 19{,}73 \times TM2 - 8{,}81 \times TM3 - 54{,}14 \times TM4 + 18{,}17 \times TM5 - 12{,}15 \times TM6 + 47{,}36 \times TM7)$	0.94	0.11

5.5 Thematic maps of Secchi Disk

The algorithm previously developed and validated for the estimation of Secchi disk was applied to every available Landsat surface reflectance image. Because of the huge number of Landsat 5 images and therefore SD maps, in Figure 24 are presented only six dates for the pit ponds located in the central area of the study area, where El Campillo, Las Madres and El Porcal are situated.

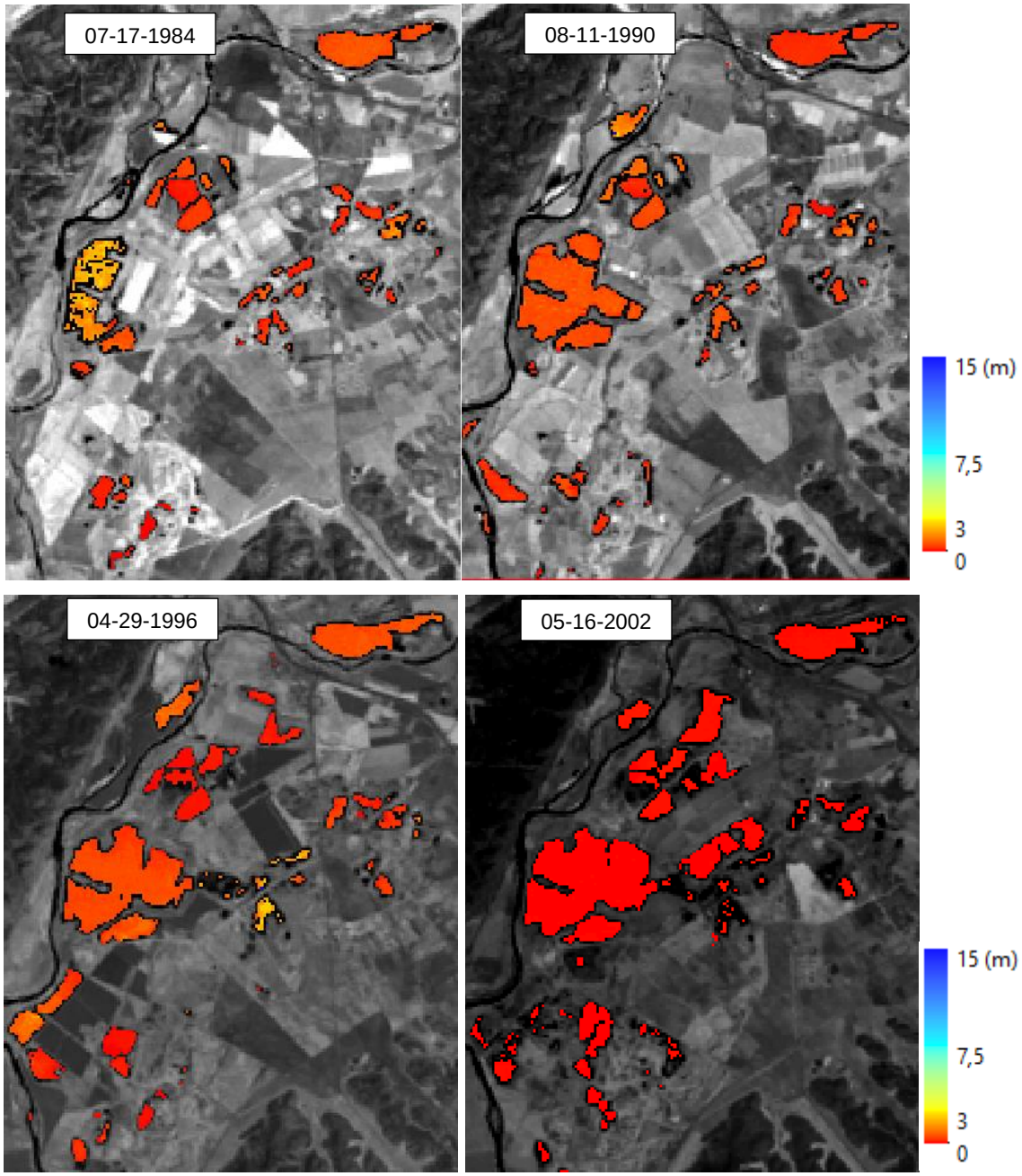
07-17-1984
08-11-1990
15 (m)
7,5
3
0
04-29-1996
05-16-2002
15 (m)
7,5
3
0

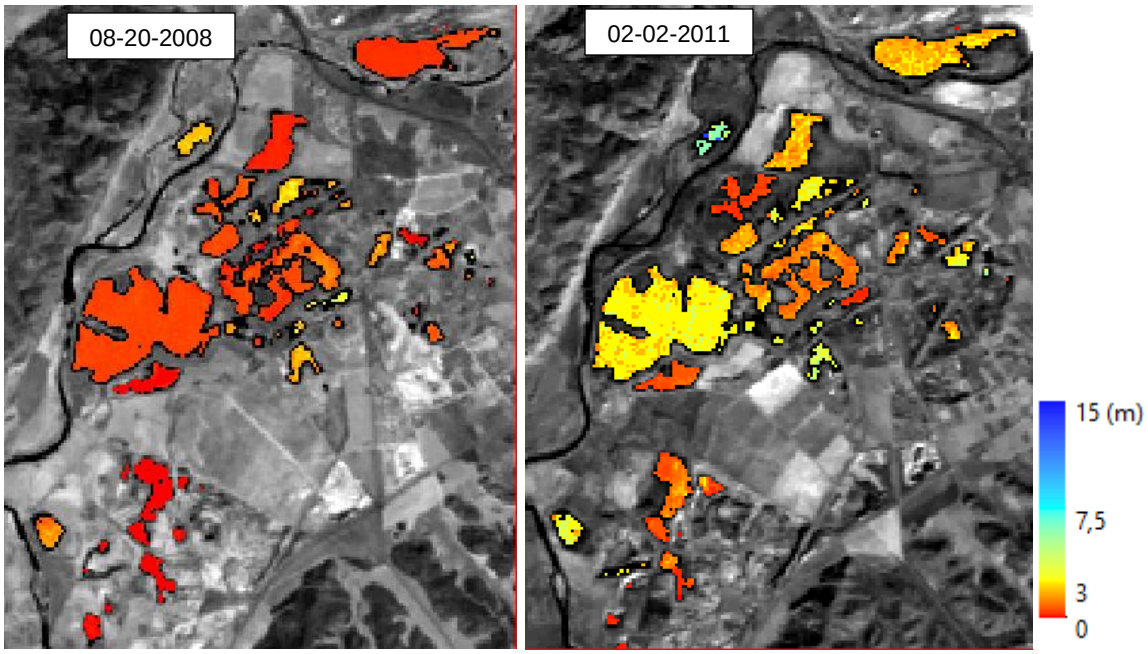

Figure 24. Thematic maps of Secchi disk for some pit ponds in the central area of PRSE, in six different dates.

In order to analyze, the Secchi disk result along the studied time series, the strategy used was to extract the minimum, maximum, mean and standard deviation of Secchi disk from the water bodies, previously radiometrically masked as water in the images (Figure 26).

In Figure 25, it is possible to identify a seasonal behavior, where the highest SD values are present in the winter (January and December) while the lowest values during summer (August). That behavior matches the phytoplankton growth, which shows unimodal cycles with summer peaks because relaxation of nutrient limitation, at the same time related with temperature and water stratification seasonality (Cebrià̀n & Valiela, 1999; Torremorell, et al., 2007; Wu, et al., 2015).

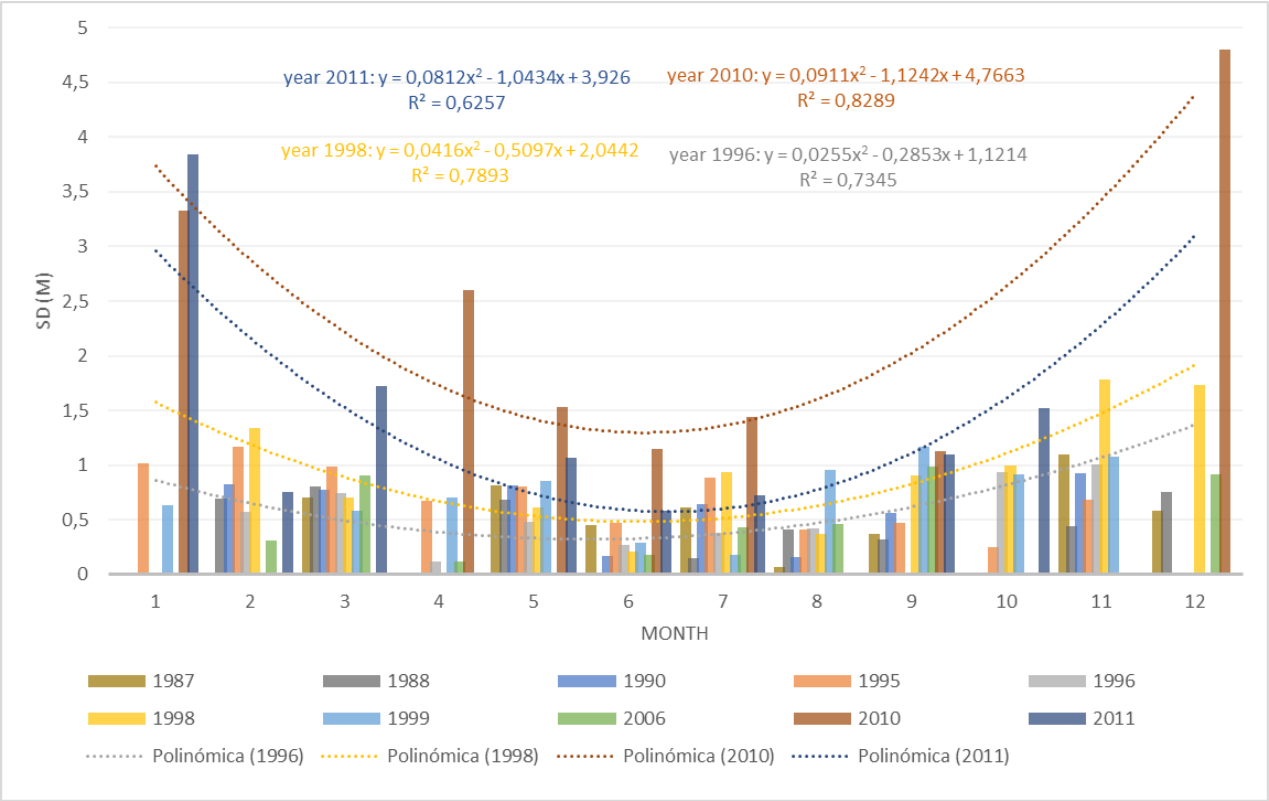

Figure 25. Monthly mean of Secchi disk.

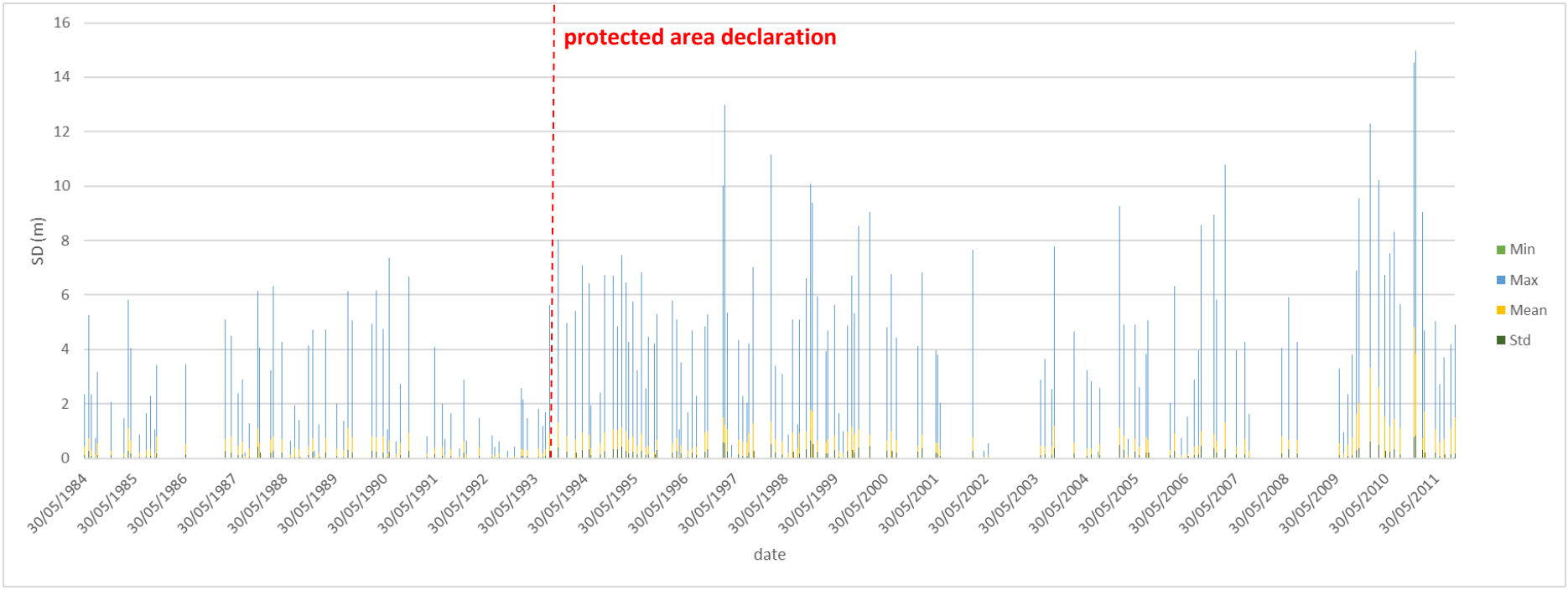

Figure 26. Monitoring of the minimum, maximum, mean and standard deviation of the Secchi disk.

5.6 Inventory of water bodies in the natural park from 1984 to 2011.

The number of water bodies assessed for each time period ranged from 29 in ~1987 to ~150 in ~2001. Because the image processing procedure targeted clear imagery and open-water areas, some water bodies were not assessed in a given time period. The main reason for some water bodies not being assessed was pervasive presence of aquatic vegetation in wetlands and shallow lakes resulting in insufficient unaffected pixels for accurate water clarity assessment. Other reasons included severe phytoplankton blooms (floating mats of phytoplankton were masked off since their spectral characteristics are more similar to green vegetation than water), and clouds or haze (Olmanson, et al., 2008).

According to Figure 27 and Figure 28, the water bodies area had an increasing period from 1984 to 2006 reaching values of 400 hectares, then the area decreased reaching values of 250 hectares. In Figure 29, it is also visible the increase of area over the years but is not visible any seasonal trend. These results are coherent with Domínguez, (2002) where identified an increase in the water sheet during the 20th century, especially in the southern area of the park, due to mining activity.

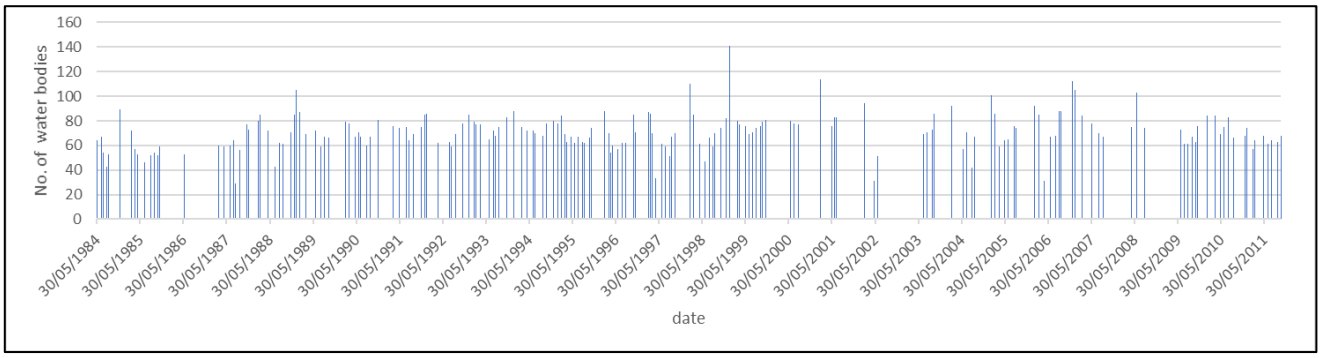

Figure 27. Number of water bodies over the studied time series.

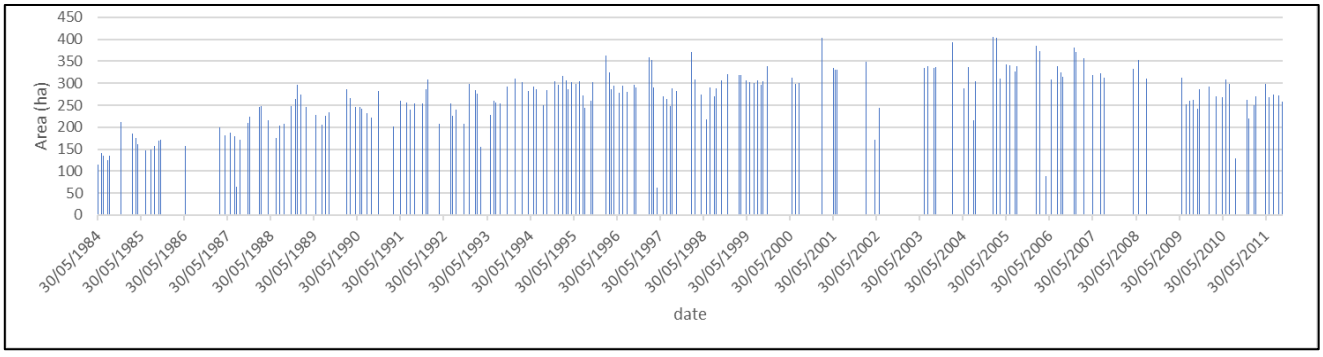

Figure 28. Area of water bodies over the studied time series.

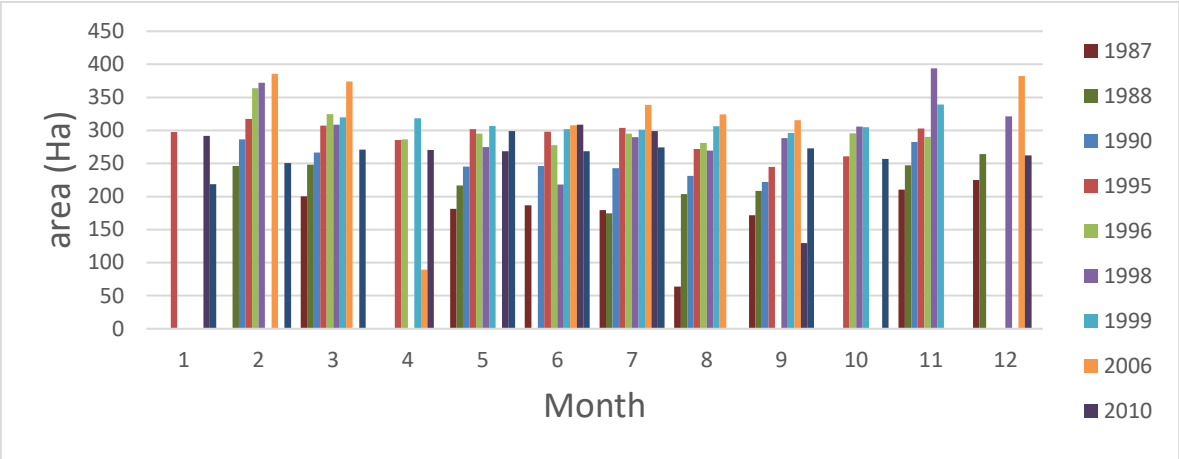

Figure 29. Monthly variation of area

It is visible the apparition of news water bodies in the nominated zone of ordered exploitation of Natural Resources which is the area constituted by lands of lower ecological quality and located on the right bank of the Jarama river, bellow the confluence of the Manzanares and Jarama Rivers (Figure 30).

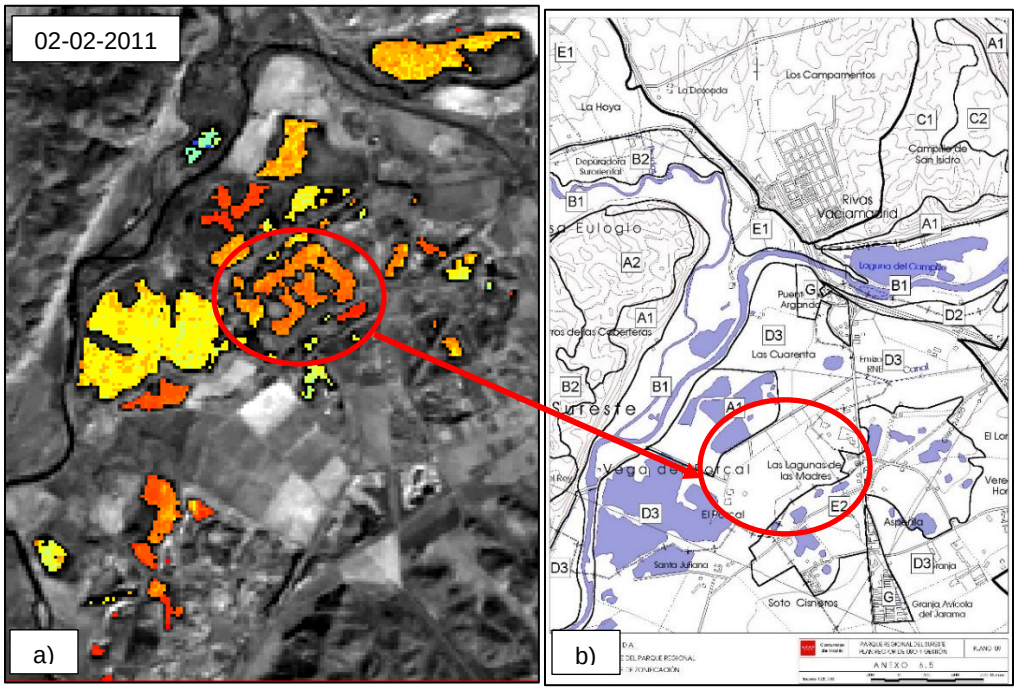

Figure 30. New water bodies appearing in Zone D. A) Retrieved SD image. B) Zonification map[7]

[7] http://www.parqueregionalsureste.org/es/zonificacion-es/textos/309-zonas-d

5.7 Identification of the trophic state of the water bodies based on the OECD classification

Having evaluated the accuracy of the obtained Secchi disk values for the entire population of water bodies for periods from 1985 to 2011, it is possible to investigate spatial patterns and temporal trends of Secchi disk. The annual mean Secchi disk map is the mean of all the resulting thematic maps (epigraph 5.5) in the same year. Then, each annual mean SD map is classified according to Table 1.

In figure 31 it is visible that most of water bodies are classified in hypereutrophic state. However, it is also evident the improvement of water quality over the years, showing 60% of water bodies in Hypereutrophic state, 30,7% in Eutrophic state and 9,3% in Mesotrophic state in year 2011. In Figure 32 is shown the map of OECD classification of water bodies trophic state (according to their SD) in 2011.

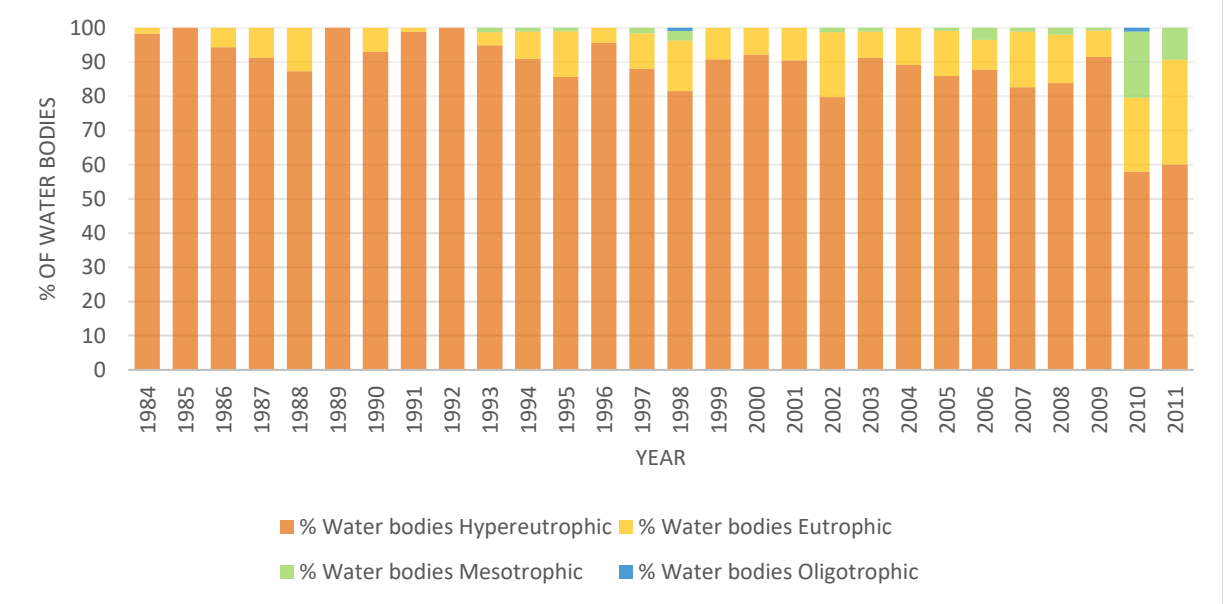

Figure 31. OECD classification of water bodies trophic state (according to their SD) from 1984 to 2011.

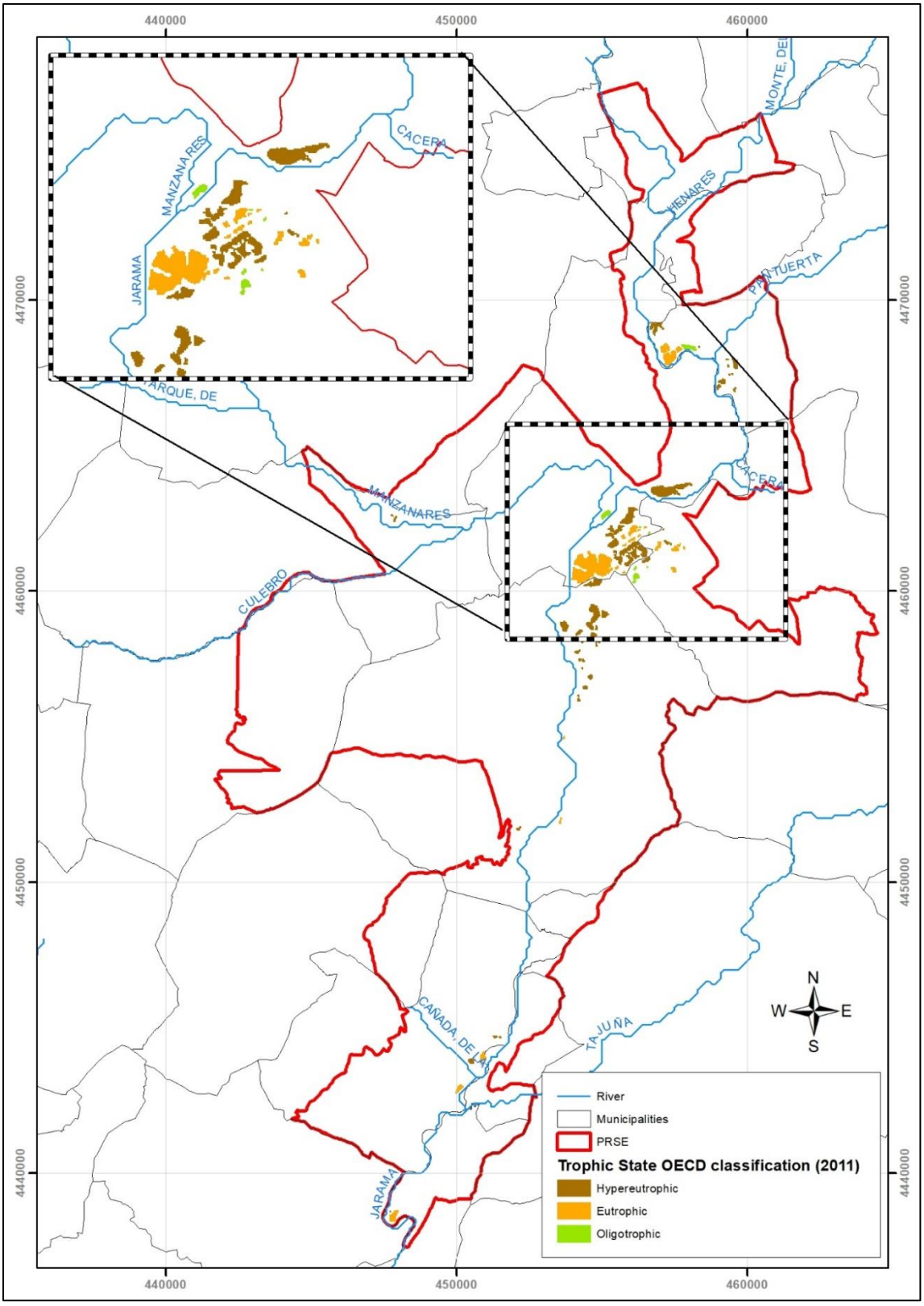

Figure 32. PRSE water bodies trophic state in year 2011 according to OECD classification

5.8 Monitoring of the ecological status of water bodies according to the WFD

Like the trophic state of the water bodies based on the OECD classification, also the annual mean Secchi disk map was used to compute the EQR as the deviation from the reference condition established as 5 meters, and finally classified. The results (Figure 33 and Figure 34) are similar to those obtained in the trophic state, where the majority of water bodies are classified in bad ecological state, but it is also visible an improvement in the last years: 45,3% in bad state, 29,3% in poor state, 16% in moderate state, 8% in good and 1,4% in high state in 2011. On 2011, the half of water bodies have improved the EQR, going from bad state in 1984 to poor, moderate, good and high in 2011. Also, in 2010 and 2011 the numbers of water bodies in good and high ecological status has increased, which demonstrates the results of changes in the water management policy and practices routed to the final objective of the WFD of "good water status" by the year 2015.

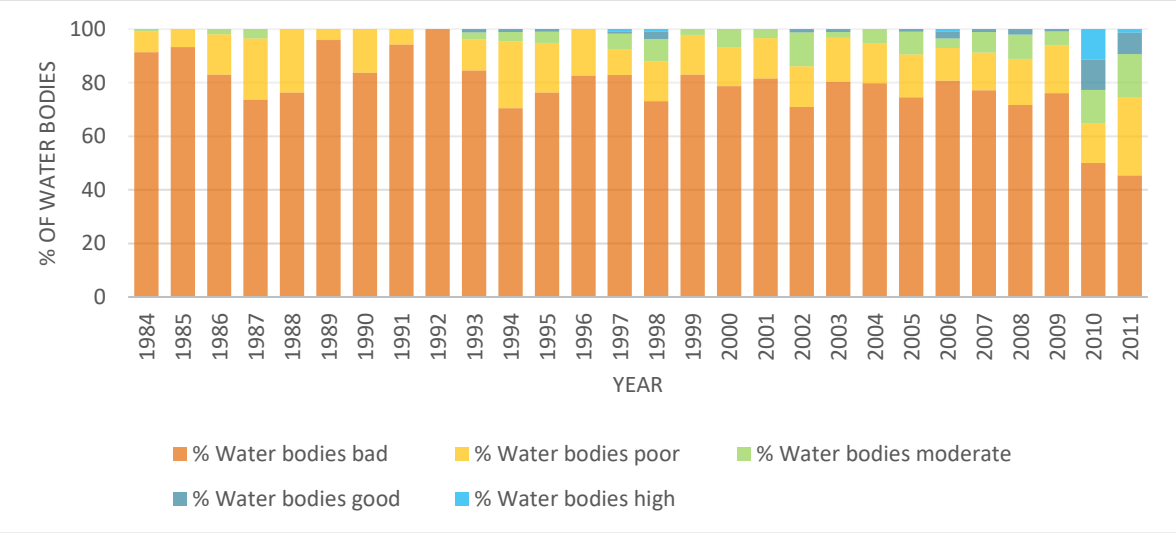

Figure 33. Ecological Quality Ratio (EQR) of water bodies from 1984 to 2011.

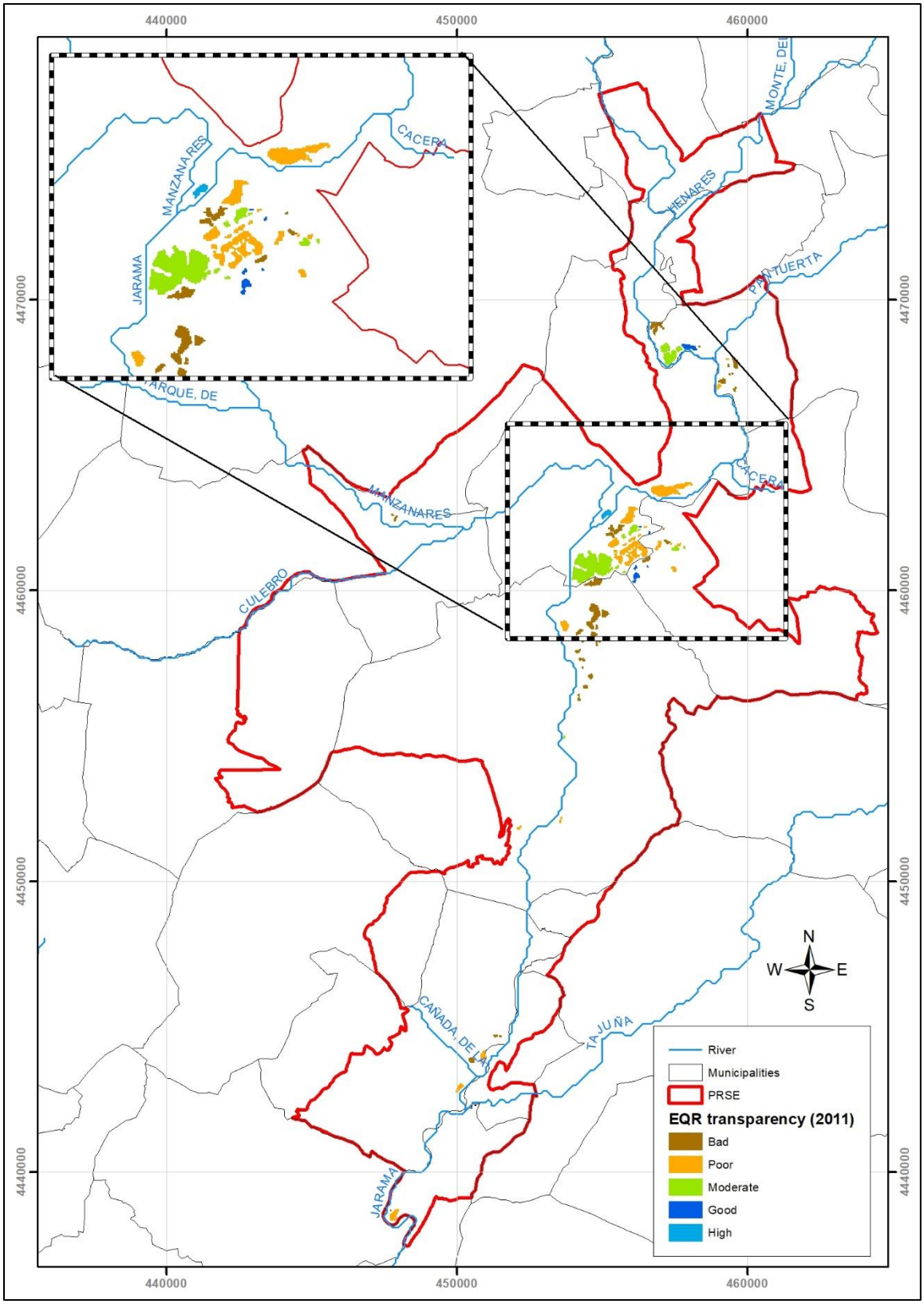

Figure 34. Ecological Quality Ratio (EQR) transparency map in year 2011.

5.9 Developing of WebGIS with Ecological Quality Ratio (EQR) and Trophic state maps

A WebGIS has been developed using GeoServer and Leaflet to visualize the obtained EQR and Trophic state for every year (Figure 35).

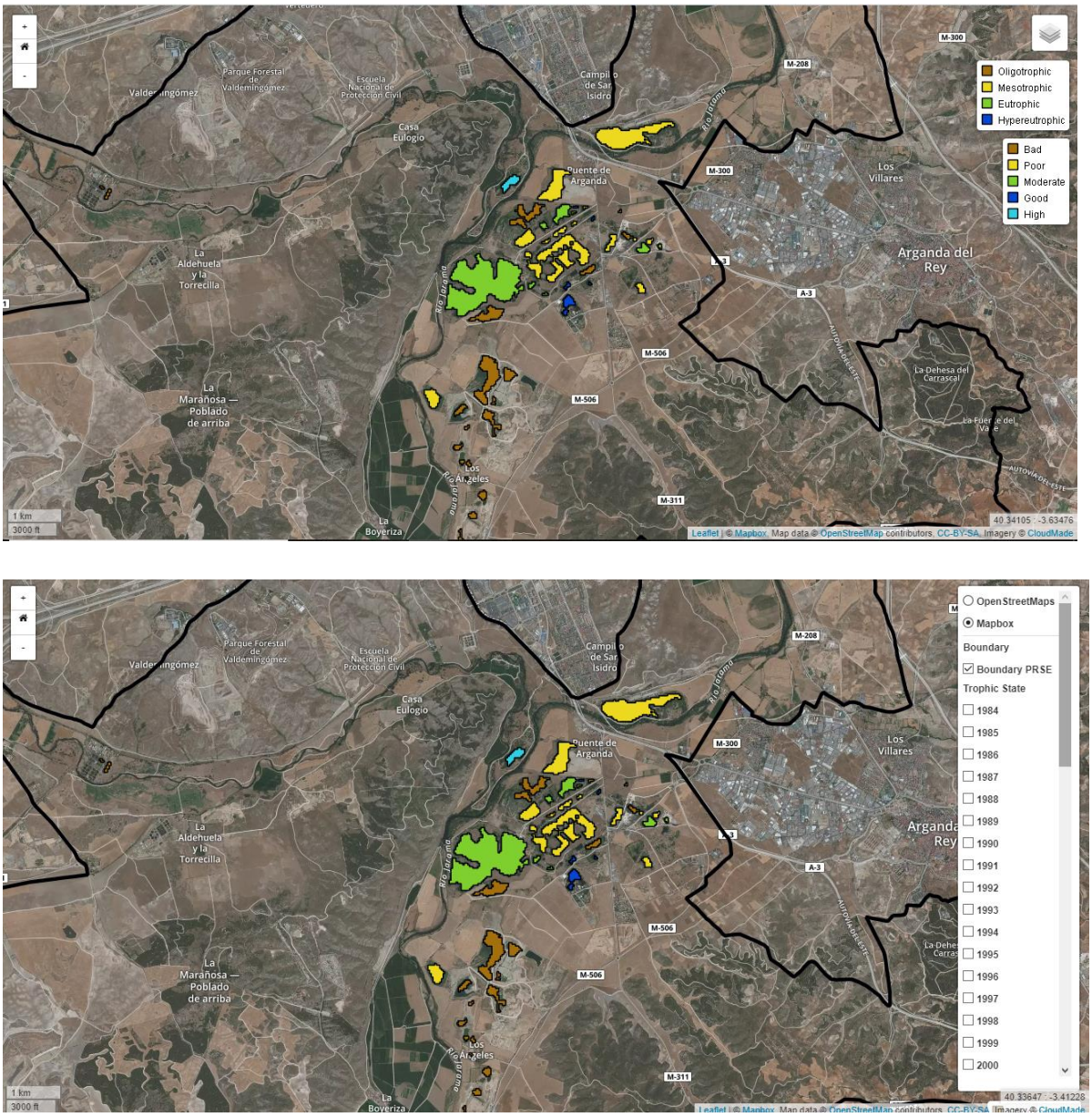

Figure 35. WebGIS

6 CONCLUSIONS

The Surface Reflectance data product produced from LEDAPS by the USGS has been compared with reflectance spectra measured in the different water bodies. The measured reflectance has values near to 1% to 5% given that water has almost no reflection in the near infrared range. Also, under most circumstances, over 90% of the light reaching a satellite over an aquatic target derives from the atmosphere. Therefore, the largest potential source of error and uncertainty in measuring from space is the residual error from atmospheric correction.

The comparison presents a qualitative consistence between the Landsat surface reflectance spectra, but using clearly defined metrics (accuracy, precision and uncertainty) and consistent graphical representation, the results indicate a large deviation from 1:1 line with a small R^2, due to the significantly overestimated Landsat surface reflectance. Thus, we had two options: to adapt the atmospheric correction to the reflectance field data or to generate a new algorithm for the Landsat surface reflectance images atmospherically corrected by LEDAPS. We chose this second option because all the Landsat 5 images have been corrected with this method, developing an algorithm to determine the SD for waters in which there is only phytoplankton, such as gravel pit ponds.

Despite the results of the comparison of remote sensing reflectance and reflectance field data show low performance, when comparing the remote sensing reflectance and Secchi disk field data to retrieve a SD algorithm, the results expose an acceptable correlation between SD and Landsat surface reflectance. To apply the obtained model to Landsat 5 surface reflectance images around the world with similar condition water bodies i.e. inland water bodies without bottom influence, it should be assessed, given the overestimation of Landsat surface reflectance.

The structure of the project is a traditional structure on water quality using remote sensing: the first step is to distinguish water and non-water information, thus three different methods have been assessed, concluding that the best performance was obtained with the NDWI, given that it has the ability of extracting more water body related information, while MNDWI and histogram thresholding mistakenly extract some small shadow and errors in the images, which presents a limitation for the extraction of small water bodies.

From these obtained water images, the evolution of water bodies has been determined, and according to the results, the area composed by water bodies in PRSE had an increasing

period from 1984 to 2006 reaching values of 400 hectares, where it is visible the apparition of news water bodies in the nominated zone of ordered exploitation of Natural Resources which is the area constituted by lands of lower ecological quality and located on the right bank of the Jarama river, bellow the confluence of the Manzanares and Jarama Rivers. That increasing trend changed from 2006, when the area decreased reaching values of 250 hectares, but it is not visible any seasonal trend.

The second step is to generate thematic maps. Once the SD maps have been generated from 1984 to 2011, we observe how the transparency varies seasonally and throughout the whole time series. The outcomes allow us to identify a SD seasonal behavior, where the highest SD values are present in the winter (January and December) while the lowest values during summer (August), which corresponds with the phytoplankton growth.

Finally, for effective environmental management, it is essential to have long-term water quality information on a broad regional and spatial scale. Development and evaluation of a 27-year water transparency, trophic state and EQR census of over 100 lakes in PRSE has demonstrated that satellite imagery allow to obtain comprehensive spatial and temporal coverage of a key water quality characteristic, given that *in situ* monitoring of lakes is usually limited to just a few point samples that may misrepresent spatially heterogeneous lakes, but the use of satellite images allows whole-lake monitoring.

The comprehensive water transparency database can be used to analyze spatial patterns and temporal trends in lake quality throughout the state and develop better understanding of the factors that affect these patterns and trends. Results of such analyses will aid managers in making informed decisions about development policy and improve the management of lake resources

It is also important to make the results easily available to lake managers, government agencies and the public. To make the data available, a web application has been created, as results of this work, where the developed EQR and trophic state maps of water bodies in PRSE, can be visualized.

The Landsat 5 finished to get images in 2013 and has been replace by Landsat 7 in 1999 and Landsat 8 in 2013 with recent technological advances. In 2015 the European Space Agency’s successfully launched Sentinel-2A into orbit, which is a system with higher frequency of image acquisition of 2-3 days at mid-latitudes and 13 bands in visible and Near-

Infra-Red (VNIR), where the main visible and near-infrared bands have a spatial resolution of 10 meters. Accordingly, the already used massive 29-year archive of Landsat 5 imagery, in future studies can be completed with Sentinel images which improves monitoring of water resources, given its higher spatial and temporal resolution.

This work has exposed once again that remote sensing is a tool for water management, also allowing the study of time series in order to generate predictive models and better understand the aquatic environment.

8 BIBLIOGRAPHY

Dekker, A. G. & Peters, S., 1993. The use of the Thematic Mapper for the analysis of eutrophic lakes: a case study in the Netherlands. *International Journal of Remote Sensing,* Volume 14, pp. 799-821.

Adler-Golden, S. M. et al., 1999. Atmospheric correction for shortwave spectral imagery based on MODTRAN4. *Imaging Spectrometry V,* Volume 3753, p. 61–69 .

Alvarez Cobelas, M. et al., 2000. *Estudio físico-químico de los ambientes estancados del Parque Regional del Sureste de la Comunidad de Madrid,* Madrid: Centro de Investigaciones Ambientales de la Comunidad de Madrid “Fernando González Bernáldez”.

Asociación Ecologista del jarama "El Soto", 2001. *Guía de humedales del Parque Regional del Sureste,* Mejorada del Campo: Asociación Ecologista del jarama "El Soto"..

Bakker, W. et al., 2009. *Principles of remote sensing for Geoinformation Science and Earth observation.* 4 ed. Enschede: International Institute.

Bernardo, N., Watanabe, F., Rodrigues, T. & Alcântara, E., 2017. Atmospheric correction issues for retrieving total suspended matter concentrations in inland waters using OLI/Landsat-8 image. *Advances in Space Research,* 59(9), pp. 2335-2348.

Boucher, J., Weathers, K., Norouzi, H. & Steele, B., 2018. Assessing the effectiveness of Landsat 8 chlorophyll a retrieval algorithms for regional freshwater monitoring.. *Ecological Applications,* 28(4), p. 1044–1054.

Cao, Z. et al., 2018. Evaluation of the sensitivity of China's next-generation ocean satellite sensor MWI onboard the Tiangong-2 space lab over inland waters. *Int J Appl Earth Obs Geoinformation,* Volume 71, pp. 109-120.

Cebriàn, J. & Valiela, I., 1999. seasonal patterns in phytoplankton biomass in coastal ecosystems. *Journal of plankton research,* 21(3), p. 429–444.

Chao Rodríguez, Y. et al., 2014. Using Landsat image time series to study a small water body in Northern Spain. *Springer,* 186(2).

Chavez, P. S., 1996. Image Based atmospheric corrections. Revisited and improved.. *Photogrammetric Engineering and remote sensing,* 62(9), p. 1025–1036.

Claverie, M., Vermote, E. F., Franch, B. & Masek, J. G., 2015. Evaluation of the Landsat-5 TM and Landsat-7 ETM+ surface reflectance products. *Remote Sensing of Environment,* Volume 169, pp. 390-403.

Dekker, A. G., Vos, R. J. & Peters, S., 2001. Comparison of remote sensing data, model results and in situ data for total suspended matter (TSM) in the southern Frisian lakes. *Science of The Total Environment,* 268(1–3), pp. 197-214.

Domínguez Gómez, J. A., Chuvieco Salinero, E. & Sastre Merlín, A., 2009. Monitoring transparency in inland water bodies using multiespectral images. *International Journal of Remote Sensing ,* pp. 1567-1586.

Domínguez Gómez, J. A. & Peña, R., 1999. Trophic state assessment in two gravel pits (El Campillo & Porcal) using airborne imagery. *Limnetica,* pp. 107-113.

Dominguez Gòmez, J. A., Sastre Merlìn, A. & Peña Martìnez, R., 1997. *Detecciòn de cambios en los humedales del rìo Jarama entre 1988 y 1992 y evaluaciòn del estado tròfico de las lagunas del Campillo, El Porcal y las Madres en 1992 mediante imàgenes Landsat TM..* Santiago de Compostela., Universidad Santiago de Compotela- Asociaciòn Española de teledetecciòn., pp. 339-351.

Domínguez, J. A., 2002. *Estudio de Calidad del Agua de lagunas de gravera mediante teledetección,* Alcalá de Henares: Universidad de Alcalá.

Domínguez, J. A., Vargas, J., Navarro, E. & Martín, A., 2017. *de la Calidad Seguimiento de la Calidad del Agua del embalse de Picadas mediante imágenes Landsat 8 (Sept. 2015 - Dic. 2016).* Murcia, Nuevas plataformas y sensores de teledetección. XVII Congreso de la Asociación Española de Teledetección..

Doña, C. et al., 2014. Empirical Relationships for Monitoring Water Quality of Lakes and Reservoirs Through Multispectral Images. *IEEE Journal of selected topics in applied earth observations and remote sensing,* 7(5), pp. 1632-1641.

Dörnhöfer, K. & Oppelt, N., 2016. Remote sensing for lake research and monitoring – Recent advances. *Ecological Indicators,* Volume 64, pp. 105-122.

Duru, U., 2017. Shoreline change assessment using multi-temporal satellite images: a case study of Lake Sapanca, NW Turkey. *Environmental Monitoring and Assessment,* pp. 189-385.

European Commission, 2000. *European Parliament and of the Council of 23 October 2000 establishing a framework for Community action in the field of water policy.* s.l.:Official Journal of the European Communities.

Giardino, C. et al., 2007. Assessment of water quality in Lake Garda (Italy) using Hyperion. *Remote Sensing of Environment,* Volume 109, p. 183–195.

Giardino, C. et al., 2001. Detecting chlorophyll, Secchi disk depth and surface temperature in a sub-alpine lake using Landsat imagery. *Science of The Total Environment,* 268(1-3), pp. 19-29.

Gilabert, M. A., Conese, C. & Maselli, F., 1994. An atmospheric correction method for the automatic retrieval of surface reflectance from TM images. *International Journal of Remote Sensing,* 15(10), pp. 2065-2086.

Glibert, P. M., 2017. Eutrophication, harmful algae and biodiversity — Challenging paradigms in a world of complex nutrient changes. *Marine Pollution Bulletin,* Volume 124, p. 591–606.

Govender, M., Chetty, K. & Bulcock, H., 2007. A review of hyperspectral remote sensing and its application in vegetation and water resource studies. *Water SA,* 33(2), pp. 145-152.

Guang, J., Yuchun, W. & Jiazhu , H., 2006. A model for the retrieval of suspended sediment concentrations in Taihu Lake from TM images. *Journal of Geographical Sciences,* 16(4), p. 458–464.

Hicks, B. J. et al., 2013. Hindcasting water clarity from Landsat satellite images of unmonitored shallow lakes in the Waikato region, New Zealand. *Environmental Monitoring and Assessment,* 185(9), p. 7245–7261.

Kloiber, S. M., Bauer, M. E., Brezonik, P. L. & Olmanson, L. G., 2002. A procedure for regional lake water clarity assessment using Landsat multispectral data. *Remote Sensing of Environment,* 82(1), pp. 38-47.

Kutser, T., 2012. The possibility of using the Landsat image archive for monitoring long time trends in coloured dissolved organic matter concentration in lake waters. *Remote Sensing of Environment,* Volume 123, pp. 334-338.

Lee, Z. et al., 2015. Secchi disk depth: A new theory and mechanistic model for underwater visibility. *Remote Sensing of Environment,* 169(2015), p. 139–149.

Maiersperger, T. K. et al., 2013. Characterizing LEDAPS surface reflectance products by comparisons with AERONET, field spectrometer, and MODIS data. *Remote Sensing of Environment,* Volume 136, pp. 1-13.

Masek, J. G. et al., 2006. A Landsat surface reflectance dataset for North America, 1990-2000. *IEEE Geoscience and Remote Sensing Letters,* 3(1), pp. 68-72.

Matthews, M. W., Bernard, S. & Winter, K., 2010. Remote sensing of cyanobacteria-dominant algal blooms and water quality parameters in Zeekoevlei, a small hypertrophic lake, using MERIS. *Remote Sensing of Environment,* 114(9), pp. 2070-2087.

McFeeters, S. K., 1996. The use of Normalized Difference Water Index (NDWI) in the delineation of open water features. *International Journal of Remote Sensing,* 17(7), p. 1425–1432.

Moran, S. M., Jackson, R. D., Slater, P. N. & Teillet, P. M., 1992. Evaluation of simplified procedures for retrieval of land surface reflectance factors from satellite sensor output. *Remote Sensing of Environment,* 41(2–3), pp. 169-184.

Mostaza-Colado, D., Carreño-Conde, F., Rasines-Ladero, R. & Iepure, S., 2018. Hydrogeochemical characterization of a shallow alluvial aquifer: 1 baseline for groundwater

quality assessment and resource management. *Science of the Total Environment,* Volume 639, p. 1110–1125.

Mouw, C. B. et al., 2015. Aquatic color radiometry remote sensing of coastal and inland waters: Challenges and recommendations for future satellite missions. *Remote Sensing of Environment,* Volume 160, pp. 15-30.

NASA, 2001. *Landsat 7 Science Data Users Handbook,* s.l.: s.n.

Olmanson, L. G., Bauer, M. E. & Brezonik, P. L., 2008. A 20-year Landsat water clarity census of Minnesota's 10,000 lakes. *Remote Sensing of Environment,* 112(11), pp. 4086-4097.

Oslo and Paris Commission OSPAR , 1997. *The Common Procedure for the Identification of the Eutrophication Status of the OSPAR Maritime Area.* Paris: s.n.

Padedda, B. M. et al., 2017. Consequences of eutrophication in the management of water resources in Mediterranean reservoirs: A case study of Lake Cedrino (Sardinia, Italy). *Global Ecology and Conservation,* Volume 12, pp. 21-35.

Pahlevan, N. et al., 2017. Sentinel-2 MultiSpectral Instrument (MSI) data processing for aquatic science applications: Demonstrations and validations. *Remote Sensing of Environment,* Volume 201, pp. 47-56.

Palmer, S. C., Kutser, T. & Hunter, P. D., 2015. Remote sensing of inland waters: Challenges, progress and future directions. *Remote Sensing of Environment,* Volume 157, pp. 1-8.

Patel, N. K., Singh, T. P., Navalgund, R. R. & Sahai, B., 1982. Spectral signatures of moisture-stressed wheat. *Journal of the Indian Society of Photo-Interpretation and Remote Sensing,* 10(1), p. 27–34.

Qi, J., Chen, J., Lafortezza, R. & Lin, Z., 2017. Remote sensing for ecosystem sustainability. In: *Reference Module in Earth Systems and Environmental Sciences.* s.l.:s.n., pp. 186 - 201.

Qin, P., Simis, S. G. & Tilstone, G. H., 2017. Radiometric validation of atmospheric correction for MERIS in the Baltic Sea based on continuous observations from ships and AERONET-OC. *Remote Sensing of Environment,* Volume 200, pp. 263-280.

Ren, J. et al., 2018. Remote observation of water clarity patterns in Three Gorges Reservoir and Dongting Lake of China and their probable linkage to the Three Gorges Dam based on Landsat 8 imagery. *Science of The Total Environment,* Volume 625, pp. 1554-1566.

Roblas Moreno, N. & García-Avilés, J., 1997. *Valoración ambiental y caracterización de los ecosistemas acuáticos leníticos del Parque Regional en torno a los ejes de los cursos bajos de los ríos Manzanares y Jarama,* Madrid: Consejería de Medio Ambiente y Desarrollo Regional.

Rudolph W. , P., 1986. Secchi disk science: Visual optics of natural waters. *Limnology and ocanography,* 31(5), pp. 909-926.

Shaw, J. & Nugent, P., 2013. Physics principles in radiometricinfrared imaging of clouds in theatmosphere. *European Journal of Physics,* Volume 34, p. S111–S121.

Singh, D. K. et al., 2018. Automated mapping of snow/ice surface temperature using Landsat-8 data in Beas River basin, India, and validation with wireless sensor network data. *Arabian Journal of Geosciences,* 11(6), p. 136.

Smith, V. H., Tilman, G. D. & Nekola, J. C., 1999. Eutrophication: impacts of excess nutrient inputs on freshwater, marine, and terrestrial ecosystems. *Environmental Pollution,* 100(1–3), pp. 179-196.

Søndergaard, M., Larsen, S. E., Jørgensen, T. B. & Jeppesen, E., 2005. Water Framework Directive: ecological classification of Danish lakes. *Journal of Applied Ecology,* 42(4), pp. 616-629.

Song, C. et al., 2001. Classification and Change Detection Using Landsat TM Data: When and How to Correct Atmospheric Effects?. *Remote sensing of environment,* Volume 75, p. 230–244 .

Soria, X. et al., 2017. *Uso de imágenes Landsat-8 para la estimación de la profundidad del disco de Secchi en aguas continentales.* Murcia, Nuevas plataformas y sensores de teledetección. XVII Congreso de la Asociación Española de Teledetección.

Torremorell, A., Bustigorry, J., Escaray, R. & Zagarese, H. E., 2007. Seasonal dynamics of a large, shallow lake, laguna Chascomús: The role of light limitation and other physical variables. *Limnologica - Ecology and Management of Inland Waters,* 37(1), pp. 100-108.

Vanhellemont, Q. & Ruddick, K., 2015. Advantages of high quality SWIR bands for ocean colour processing: Examples from Landsat-8. *Remote Sensing of Environment,* Volume 161, pp. 89-106.

Verdin, J. P., 1985. Monitoring water quality conditions in large western reservoir with Landsat imagery. *Photogrammetric Engineering and Remote Sensing,* Volume 51, pp. 343-353.

Vermote, E. F. et al., 1997. Second Simulation of the Satellite Signal in the Solar Spectrum, 6S: An Overview. *IEEE Transactions on Geoscience and remote sensing,* 35(3).

Vollenweider, R. A., 1968. *Scientific fundamentals of the eutrophication of lakes and flowing waters, with particular reference to nitrogen and phosphorus as factors in eutrophication,* Paris: OECD.

Vollenweider, R. A. & Kerekes, J. J., 1982. *Eutrophication of waters: monitoring assessment and control, Organization for Economic Co-operation and Development.* Paris: OECD.

Wei, J. et al., 2018. An assessment of Landsat-8 atmospheric correction schemes and remote sensing reflectance products in coral reefs and coastal turbid waters. *Remote Sensing of Environment,* Volume 215, p. 18–32.

Wei, J., Lee, Z. & Shang, S., 2016. A system to measure the data quality of spectral remote-sensing reflectance of aquatic environments. *Journal of Geophysical Research: Oceans,* 121(11), pp. 8189-8207.

Wernand, M. R., 2010. On the history of the Secchi disk. *Journal European Optical Society,* 5(100135), pp. 2-6.

Wetzel, R. G., 2001. *Limnology.* 3 ed. New York: Elsevier Inc.

Wu, Z. et al., 2015. Seasonal-Spatial Distribution and Long-Term Variation of Transparency in Xin'anjiang Reservoir: Implications for Reservoir Management. *Int J Environ Res Public Health,* 12(8), p. 9492–9507.

Xu, H., 2006. Modification of normalized difference water index (NDWI) to enhance open water features in remotely sensed imagery. *International Journal of Remote Sensing,* 27(14), p. 3025–3033.

ANNEX 1: SECCHI DISK FIELD DATA

Table 1. Secchi disk measurements developed by Domìnguez Gòmez, Sastre Merlìn, & Peña Martìnez, (1997) and Domínguez & Peña, (1999).

Point	Secchi Disk (m)
cam92-1	0,34
cam92-2	0,39
cam92-3	0,44
cam92-4	0,37
cam92-5	0,36
cam92-6	0,44
por92-1	0,2
por92-2	0,22
por92-3	0,25
por92-4	0,24
por92-5	0,26
por92-6	0,24
por92-7	0,24
mad92-1	4,44
mad92-2	4,84
mad92-3	2,69
cam97-1	0,5
cam97-2	0,48
cam97-3	0,49
cam97-4	0,63
cam97-5	0,47
cam97-6	0,32
cam97-7	0,39
por97-1	0,53
por97-2	0,6
por97-3	0,68
por97-4	0,5
por97-5	0,5
por97-6	0,57
por97-7	0,53
por97-8	0,64
mad97-1	5,73
mad97-2	3,47
mad97-3	5,72

Mad: Las Madres pond
Camp: El Campillo pond
Por: El Porcal pond

Table 2. Secchi disk measurements in July 2000 by Domínguez, (2002).

Point	Date	Secchi Disk (m)
C1	03-jul-00	1,18
C2	03-jul-00	1,22
C3	03-jul-00	1,2
C4	03-jul-00	1,21
C5	03-jul-00	1,37
C6	03-jul-00	1,13
C7	03-jul-00	1,17
C8	03-jul-00	1,25
C9	03-jul-00	1,13
C10	03-jul-00	1,11
C11	03-jul-00	1,13
C12	03-jul-00	1,13
C13	03-jul-00	1,19
C14	03-jul-00	1,01
C1	31-jul-00	1,08
C3	31-jul-00	1,03
C4	31-jul-00	1,19
C6	31-jul-00	1,04
C8	31-jul-00	1,11
M1	31-jul-00	4,09
M2	31-jul-00	4,18
M3	31-jul-00	4,3
M4	31-jul-00	4,03
M5	31-jul-00	4,24
M6	31-jul-00	4,1
M7	31-jul-00	4,02
M8	31-jul-00	4,27
M1	04-jul-00	3,32
M2	04-jul-00	3,43
M3	04-jul-00	3,34
M4	04-jul-00	3,23
M5	04-jul-00	3,46
M6	04-jul-00	3,42
P1	04-jul-00	0,75
P2	04-jul-00	0,56
P3	04-jul-00	0,54
P4	04-jul-00	0,6
P5	04-jul-00	0,64
P6	04-jul-00	0,67
P7	04-jul-00	0,71
P8	04-jul-00	0,63
P9	04-jul-00	0,66
P10	04-jul-00	0,65
P11	04-jul-00	0,65
P12	04-jul-00	0,64
P13	04-jul-00	0,63
P14	04-jul-00	0,66
P15	04-jul-00	0,64
P16	04-jul-00	0,62
P17	04-jul-00	0,58
P18	04-jul-00	0,6

M: Las Madres pond
C: El Campillo pond
P: El Porcal pond

Table 3. Secchi disk measurements by Dr. Miguel Álvarez Cobelas.

Month	1991	1992	1993	1994	1995	1996	1997	1998	1999	2000	2001
J		3,1	2,6	3,5	1,9	3,7	5,1	3,8	2,5	1,6	2,5
F		3,7	3,3	3,6	2,9	3,5	4,2	7,2	3,1	3,6	3
M		5,4	4,1	3,9	4,3	5,5	5	5,2	3,6	3,7	6
A		6,8	3,7	4,2	5,5	1,5	2,7	4,1	4,2	4	3,5
M		3	3,8	3,5	4,5	4	5	4,2	4,2	3,7	3,3
J		3	2,8	3,6	5,3	3,5	3	4	4,3	3,5	4
J		4	3,1	4	3,5	3,9	3	4	4,4	5	3,4
A		2,5	2,1	3,3	2,4	2,7	2,5	4	4,5	3,5	4,5
S	3,8	2,5	2,1	2,9	4,5	3,2	3,5	3,4	3,7	3,5	3,5
O	3,5		3	2,5	4,2	4,7	5,6	3,4	5,1	4,5	4,8
N	2,2	2,8	2,6	4	6	3,6	4,2	3,4	1,5	1,5	0,7
D	3,2	2,7	3,7	4		2,8	4	1,5	1	1,6	1,5

Month	2002	2003	2004	2005	2006	2007	2008	2009	2010	2011	2012	2013
J	3,2	1,6	1,1	1,4	0.4	1.5	1.95	1.2	1.5	1	1	3
F	3,5	1,8	1,7	1	1.1	1.9	3.20	3	2.05	1.7	1.5	1.85
M	4,5	5,1	3	2	2.5	1.5		2.3	2.5	3.2	4.6	3.85
A	5	2,7	4,2	4	3.2	2.1	2.90	2.7	2.9	5.4	5	8
M	3	4	4,5	3,7	4.8	5.5	4.30	5.6	1.5	2.3	4	4
J	4,3	3,7	5,1	3,5	3.0	4.4	4.00	2.8	5	3	4	4.8
J	3,6	3,5	4	3,5	4.0	4.5	4.20	2.5	4.4	3.5	3.5	2.2
A	3,9	3,8	4,2	4,5	3.0	2.5	4.10	5.6	5.5	3	3	2.6
S	4,2	4,5	3,4	3,1	1.8	2.5	3.40	4.1	4.15	4.3	5.5	2.6
O	3	3,1	2,2	2,8	0.5	0.3	0.30	0.4	0.8	1.4	2	3.1
N	2,2	0,8	0,6	0,5	0.5	1.0	0.90	0.4	0.4	0.4	1.8	0.52
D	1	0,8	1	0,4	1.1	1.2	1.30	1.1	0.4	0.6	1.3	0.4